Ultrasound of Skin Cancer

5

Ximena Wortsman

Contents

5.1 Introduction

The most common forms of skin cancer can be divided into melanoma and non-melanoma skin cancers. Non-melanoma skin cancers are the most frequent form of cancer in humans. Of these, basal cell carcinoma is the most common form, followed by squamous cell carcinoma. Each year there are more new cases of skin cancer than the combined incidence of cancers of the breast, prostate, lung, and colon [1, 2].

5.2 Non-melanoma Skin Cancer

5.2.1 Basal Cell Carcinoma

5.2.1.1 Definition

Epithelial malignant tumor of low malignant potential, which presents basaloid cells. It is the most common form of skin cancer and usually affects the skin exposed to the sun.

5.2.1.2 Synonyms

Basal cell epithelioma, Basalioma.

5.2.1.3 Facts on Basal Cell Carcinoma

- Of all cases of basal cell carcinoma (BCC), 85% are located in the head and neck. BCC is rarely lethal, but it may be disfiguring because it commonly involves the face. Metastases are rare [1–4].
- Ultrasound is a first-line imaging technique for studying this tumor because it can show the exact location, characteristics, and extent of the primary lesion (including thickness), without limitations in penetration [5–8].

X. Wortsman, *Atlas of Dermatologic Ultrasound*, https://doi.org/10.1007/978-3-319-89614-4_5

5.2.1.4 Key Sonographic Signs

- Oval or band-like hypoechoic dermal and/or hypodermal structure with slightly irregular borders that commonly presents hyperechoic spots. These spots have been correlated to the presence of compact nests of neoplastic cells and seem not to correspond to calcium deposits or cornified cysts (Figs. 5.1, 5.2, 5.3, and 5.4) [5–14].
- Occasionally, the tumors can show an "hourglass" or "butterfly" shape or can be lobulated, asymmetric, irregular, or bulging [8]
- The presence of seven or more hyperechoic spots within the lesion has been associated with BCC histologic subtypes having a high risk of recurrences, such as micronodular, sclerosing, infiltrating, morpheiform, and metatypical subtypes (Figs. 5.5, 5.6, and 5.7). The low risk of recurrences histologic subtypes include macronodular or nodular, superficial, adenoid cystic, and Pinkus fibroepithelioma [7].
- Occasionally, the involvement of muscles or cartilage may be detected, most often in lesions located on the nose, eyelids, ears, and lips [5–8, 10].
- On color Doppler, there is low to moderate vascularity within or at the bottom of the lesion, with low-velocity arterial and/or venous vessels [5–8, 10].
- Superficial and nodular subtypes of BCC composed of nests of cells that measure less than 0.1 mm may not show hyperechoic spots, correlating with the current limitations of the definition of the ultrasound devices working with variable frequency probes that present an upper range of 15–24 MHz [5].
- Subtypes of BCC with the high and low risk of recurrence subtypes may be detected in the same lesion. These lesions present areas with marked differences in the density of the hyperechoic spots (i.e., high and low density or number). Knowledge of this mixed type of BCC lesions can support the choice of the site of biopsy and/or the type of surgery [9].

Fig. 5.1 Basal cell carcinoma of high-risk-of-recurrence subtype. (**a**) Clinical image. (**b** and **c**), Greyscale and color Doppler ultrasound (transverse views) show 18.9-mm (transverse) × 1.8-mm (thickness) hypoechoic dermal band in the right paranasal region, suggestive of high-risk-of-recurrence subtype. Notice more than seven hyperechoic spots (*arrows*) that are seen within the lesion (histology: morpheiform). On color Doppler, there is increased vascularity within the lesion.

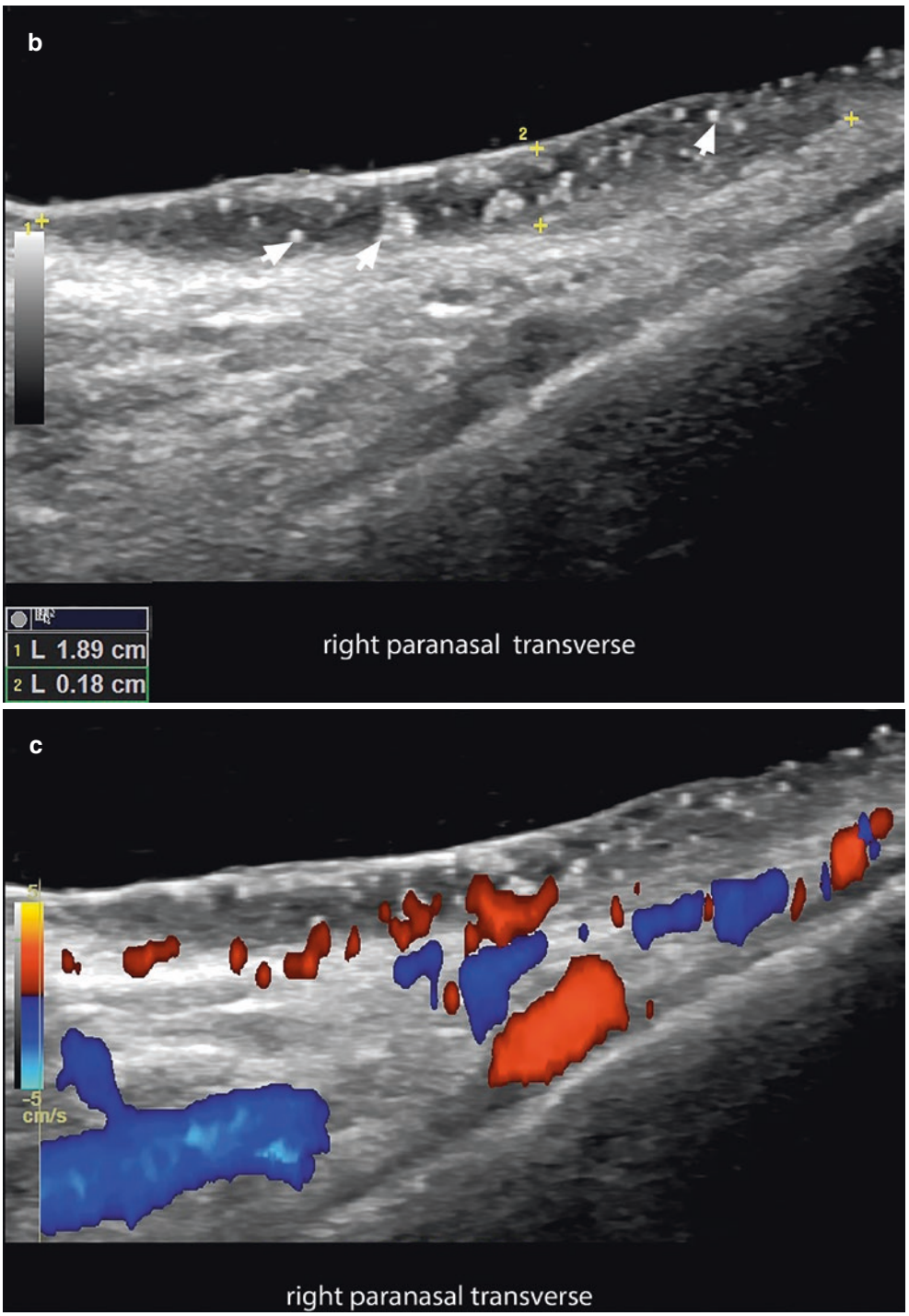

Fig. 5.1 (Continued)

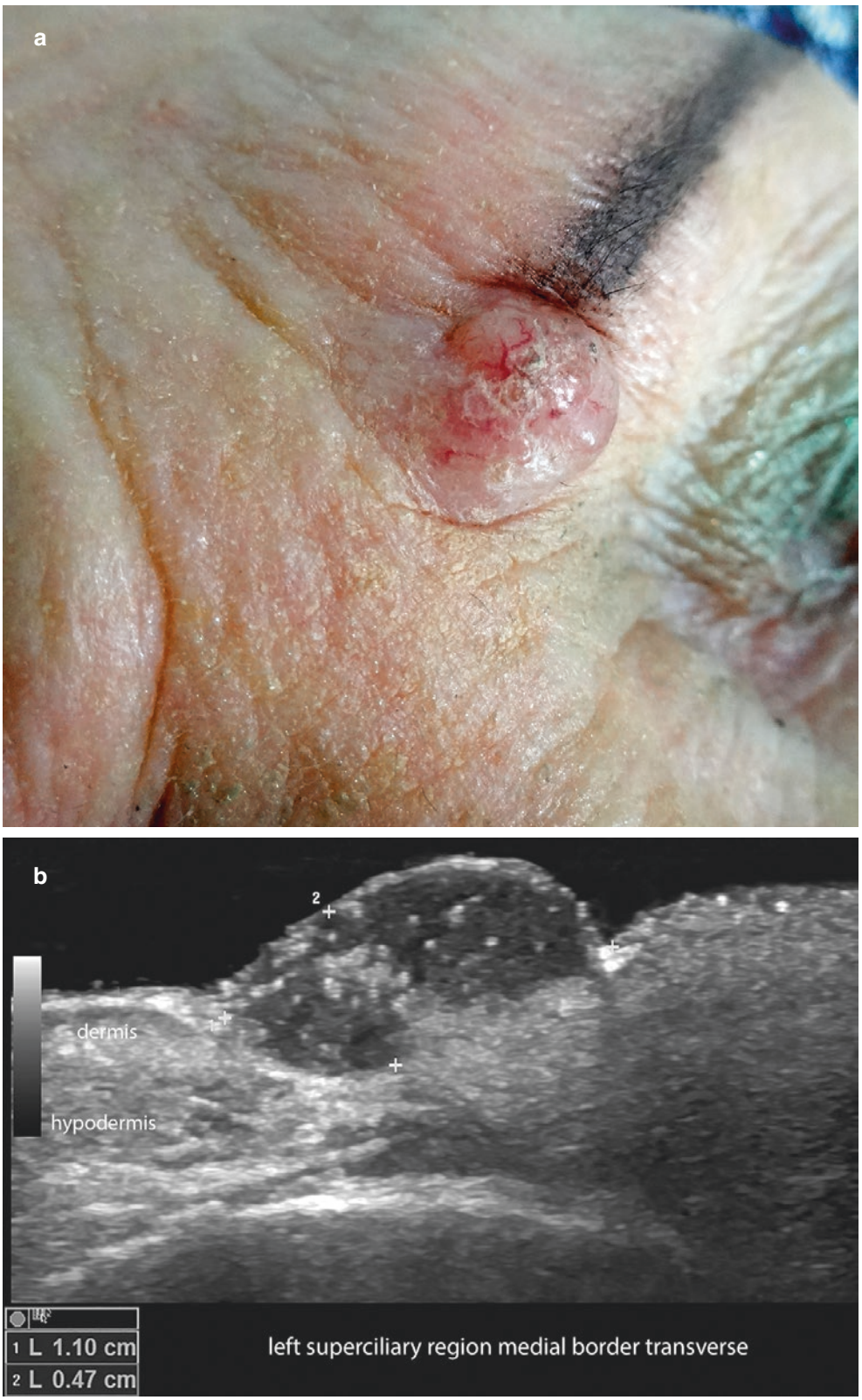

Fig. 5.2 Mixed high-risk and low-risk-of-recurrence basal cell carcinoma. (**a**) Clinical image. (**b** and **c**), Greyscale and color Doppler (longitudinal view). (**d**) 3D reconstruction ultrasound (transverse views, left superciliary region). Mixed subtypes shown in this lesion are micronodular (high risk of recurrence) and nodular (low risk of recurrence). The high-risk-of-recurrence subtype appears as areas with a higher concentration of hyperechoic spots. Color Doppler shows hypervascularity in the periphery and within the lesion, with thin arterial and venous vessels.

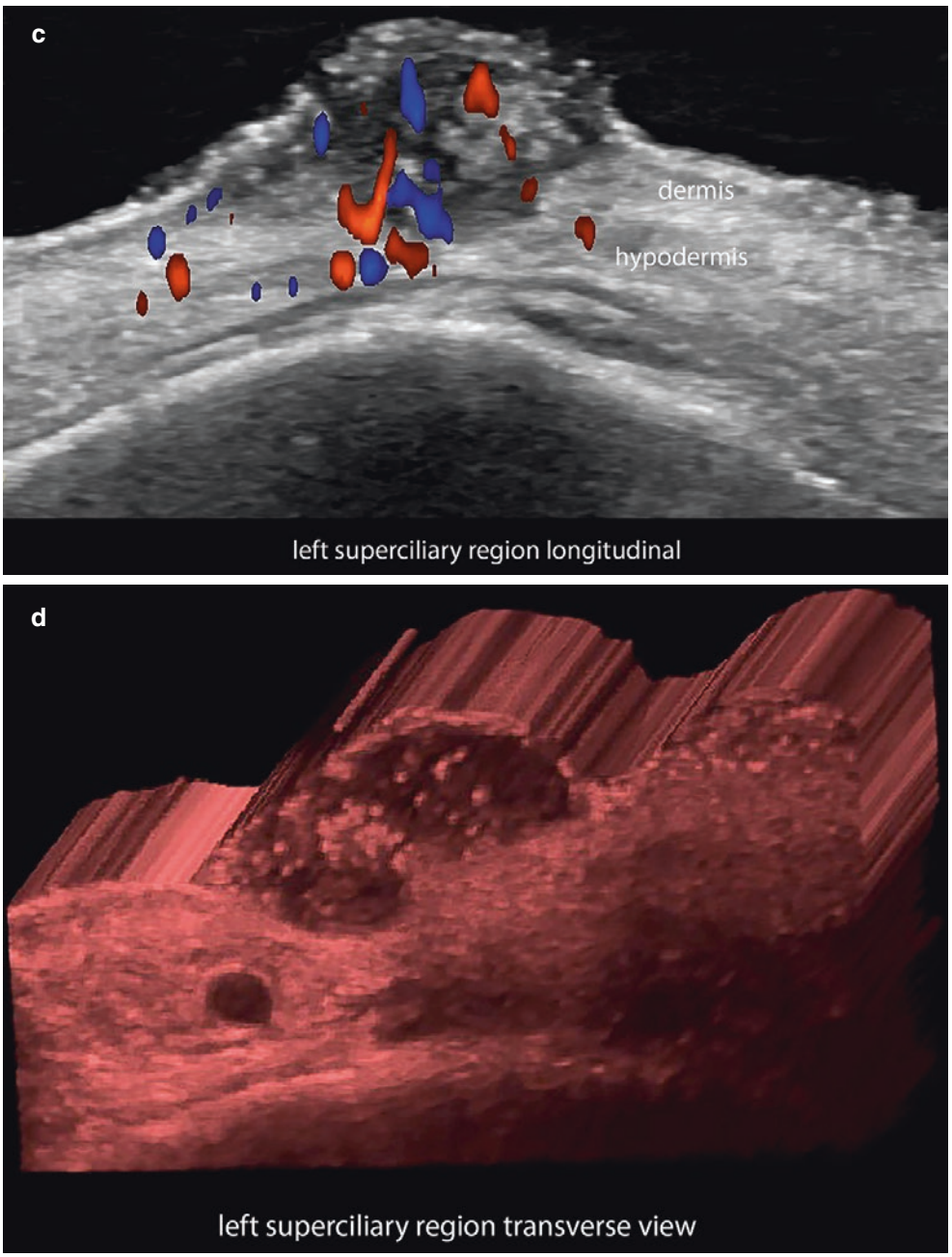

Fig. 5.2 (Continued)

Fig. 5.3 Basal cell carcinoma of low-risk-of-recurrence subtype. (**a**) Clinical image. (**b**) Greyscale. (**c**) 3D reconstruction ultrasound (transverse views; left nasal ala) demonstrate a well-defined, oval-shaped hypoechoic lesion (*asterisk*) suggestive of low-risk-of-recurrence subtype (histology: nodular subtype). Notice the small number of hyperechoic spots (*arrowheads*) within the lesion.

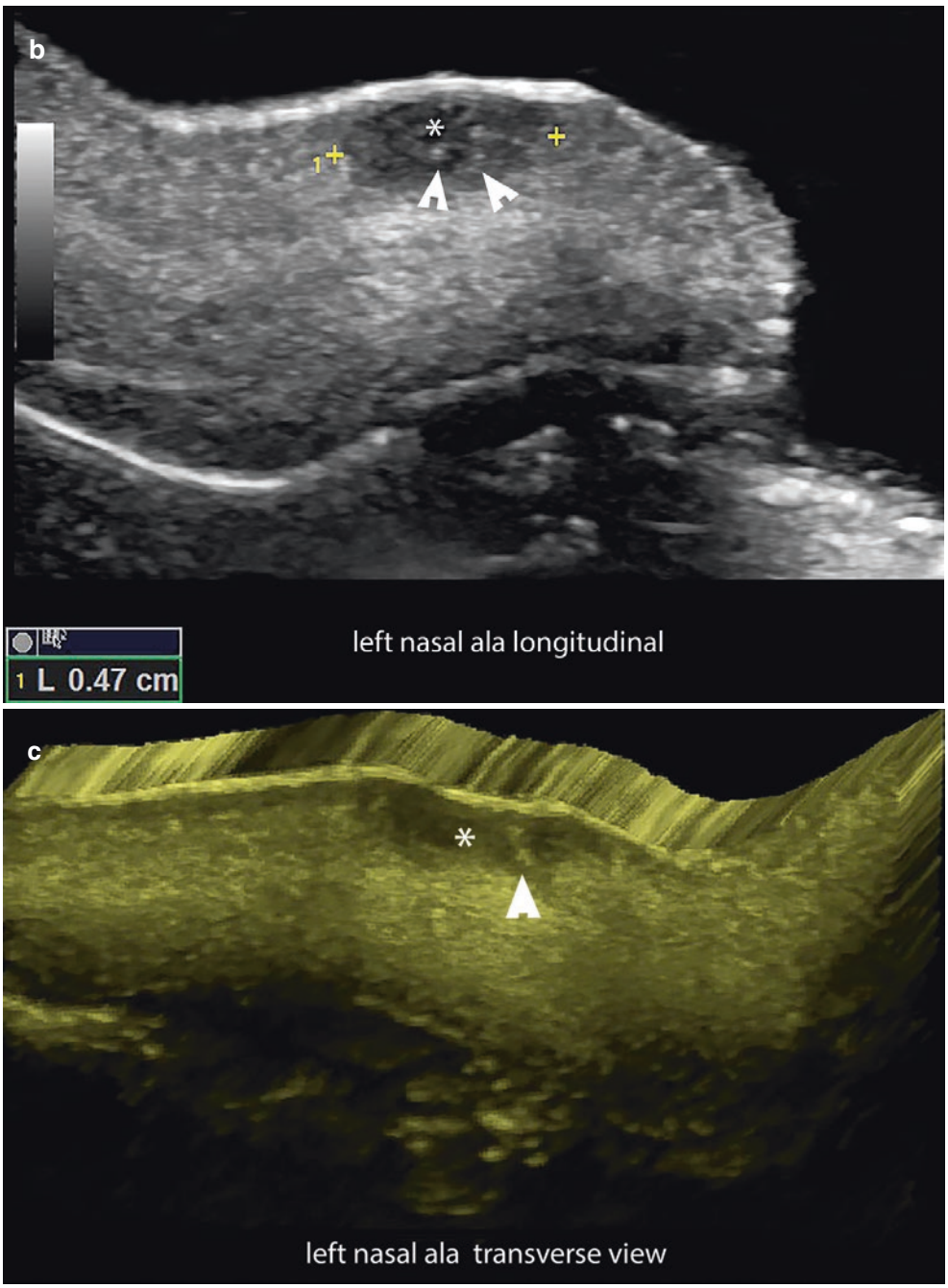

Fig. 5.3 (Continued)

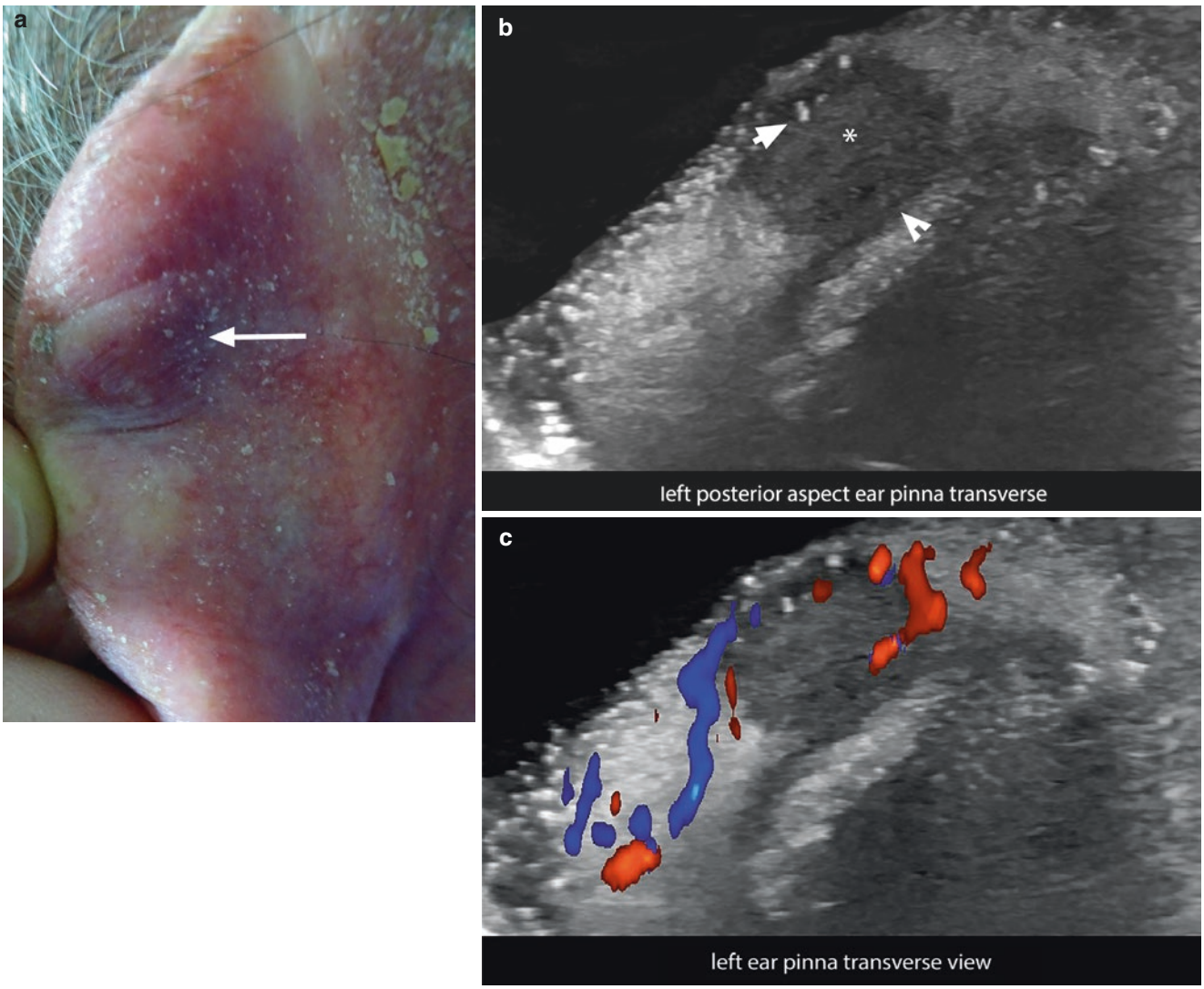

Fig. 5.4 Basal cell carcinoma of low-risk-of-recurrence subtype that involves the auricular cartilage. (**a**) Clinical image that was simulating another dermatologic lesion owing to the lump. (**b** and **c**) Greyscale and color Doppler ultrasound (transverse views; left ear pinna) show round, hypoechoic dermal structure (*asterisk*) that involves the surface of the auricular cartilage (*arrowhead*). Few hyperechoic spots (*arrow*) are detected within the lesion. On color Doppler, there is a slight increase of the vascularity, mainly in the periphery of the lesion. Histology: nodular subtype.

Fig. 5.5 Basal cell carcinoma of high-risk-of-recurrence subtype that does not involve the auricular cartilage. (**a**) Clinical photograph. (**b**) Greyscale. (**c**) 3D reconstruction ultrasound (transverse views; left ear pinna).

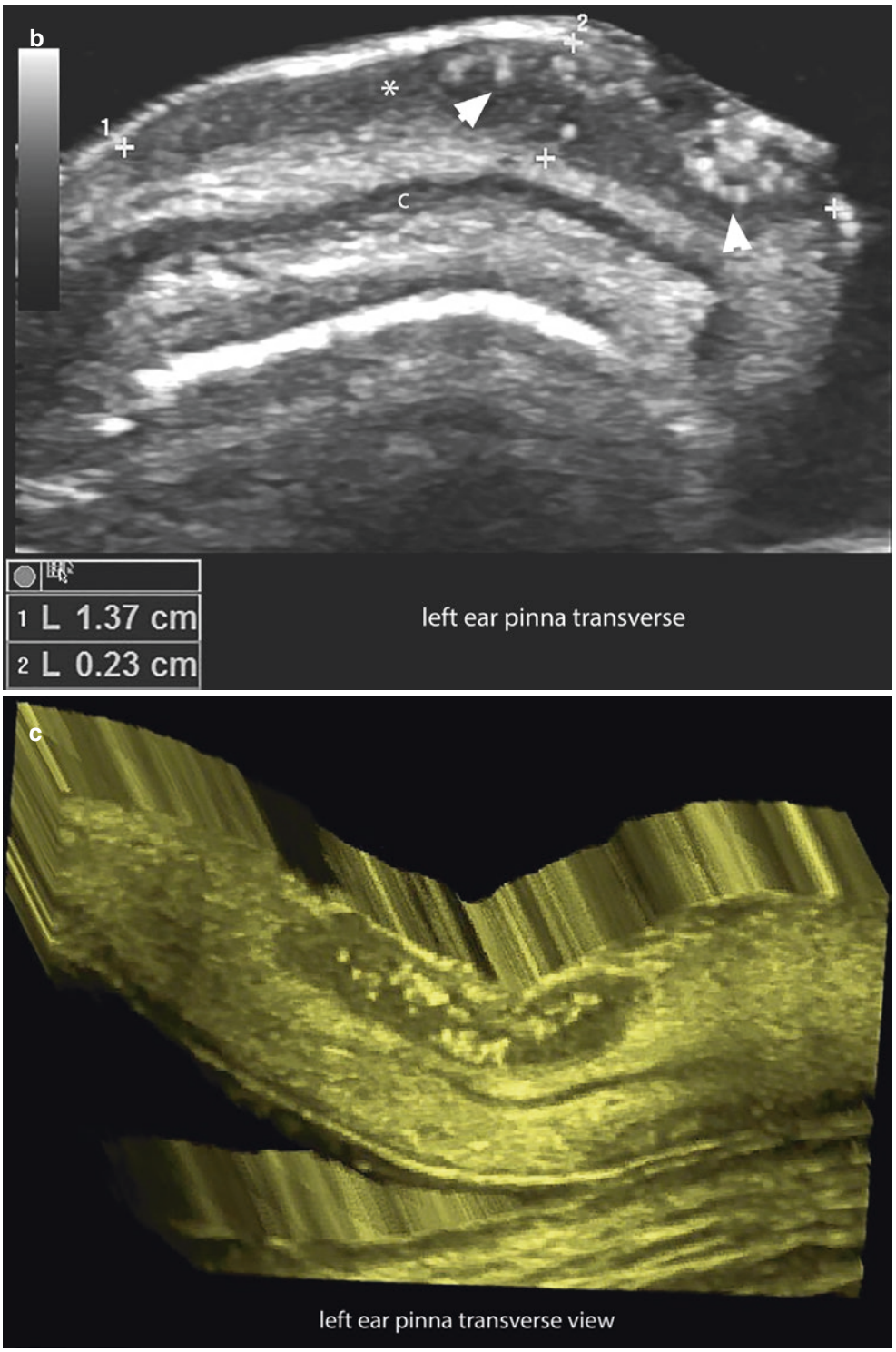

Fig. 5.5 (Continued)

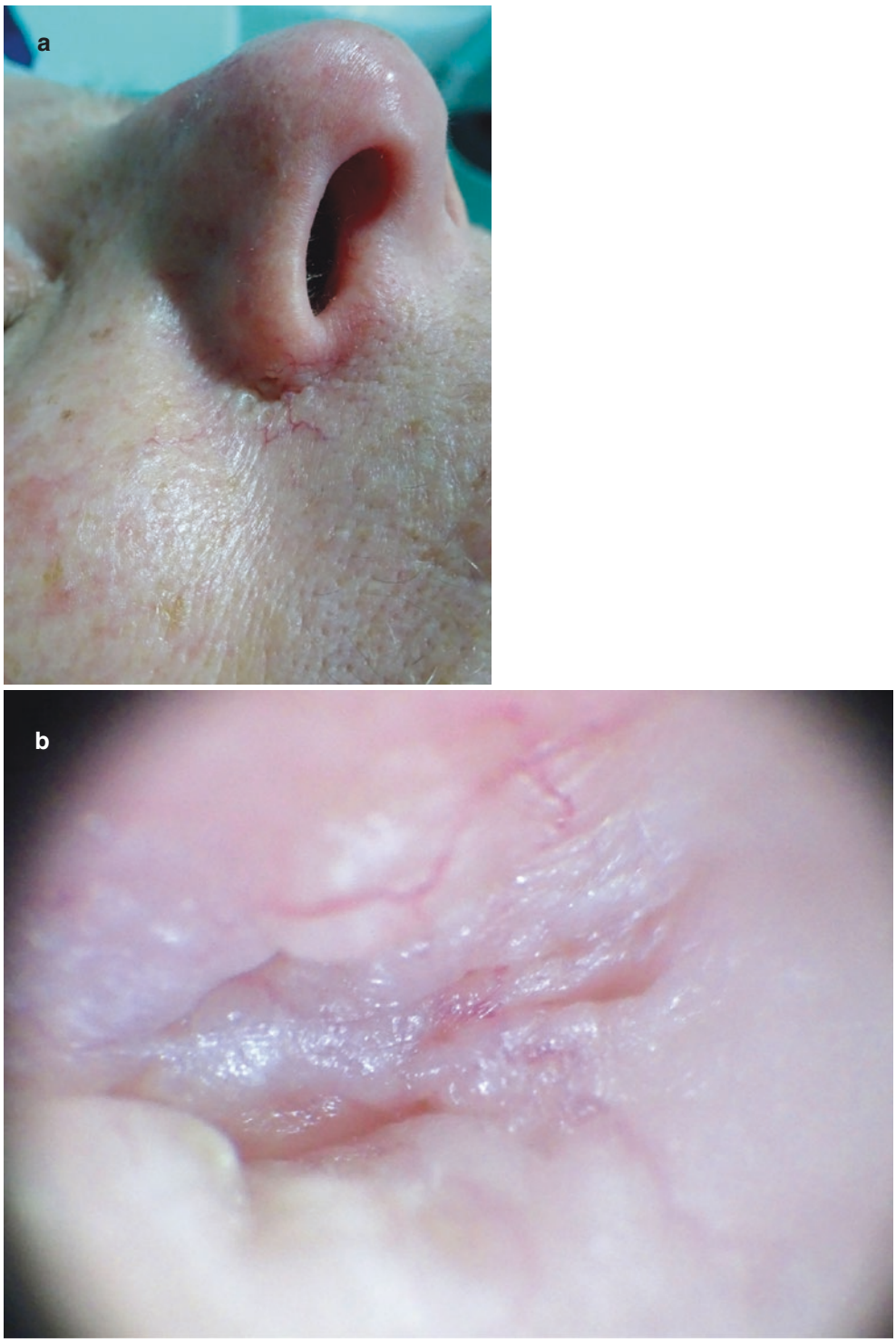

Fig. 5.6 Basal cell carcinoma of high-risk-of-recurrence subtype that involves dermis and hypodermis. (**a**) Clinical photograph. (**b**) Dermoscopic image. (**c**) Greyscale (longitudinal view; right perinasal region) and (**d**) color Doppler ultrasound (transverse view; right perinasal region) demonstrate pyramid-shaped dermal and hypodermal hypoechoic image. The vertex of the pyramid (*arrow*) is located at the deep part of the lesion. There are multiple hyperechoic spots, suggestive of a high-risk-of-recurrence subtype. On color Doppler, there is increased blood flow at the bottom of the lesion. Histology: morpheiform subtype.

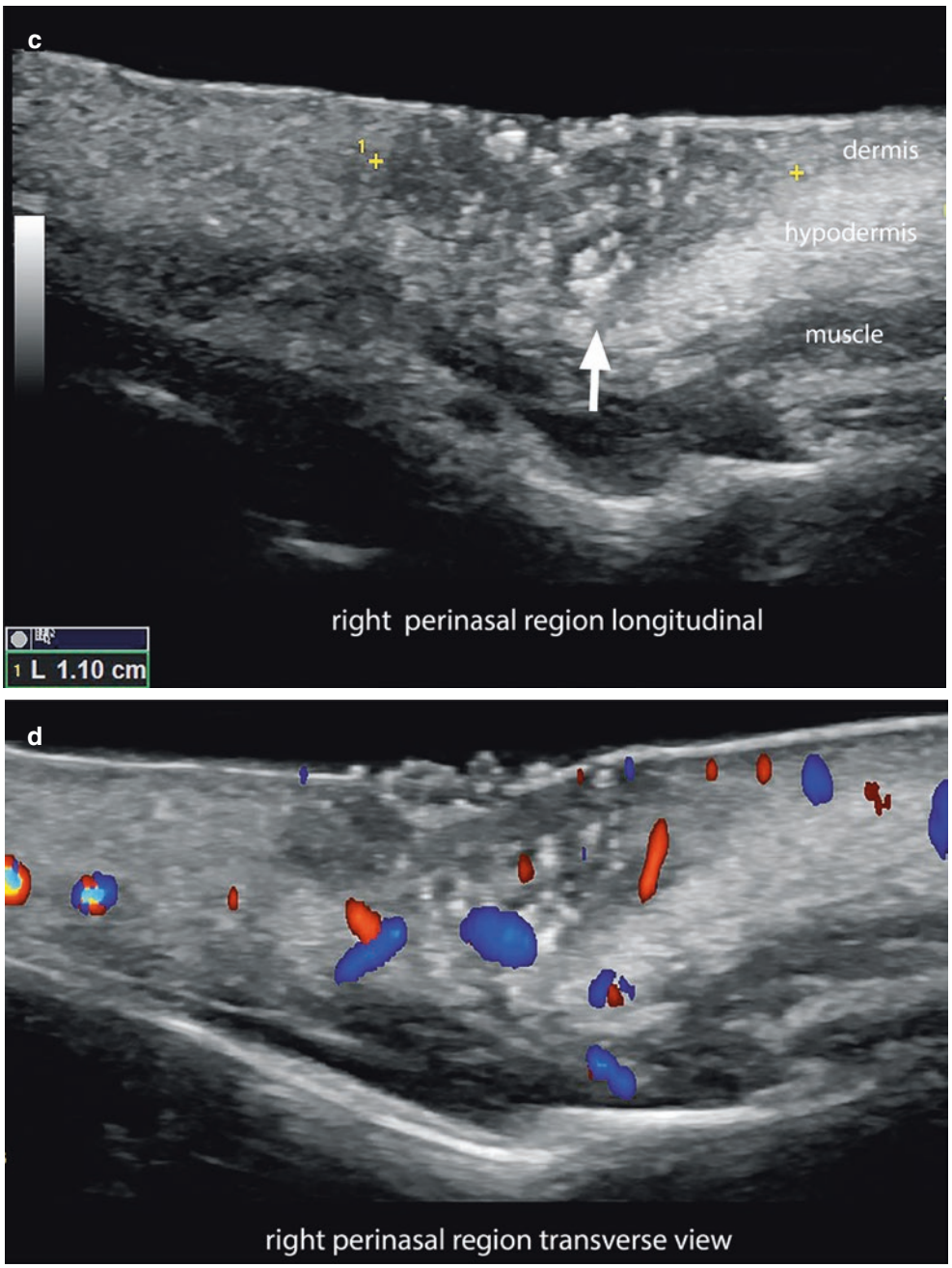

Fig. 5.6 (Continued)

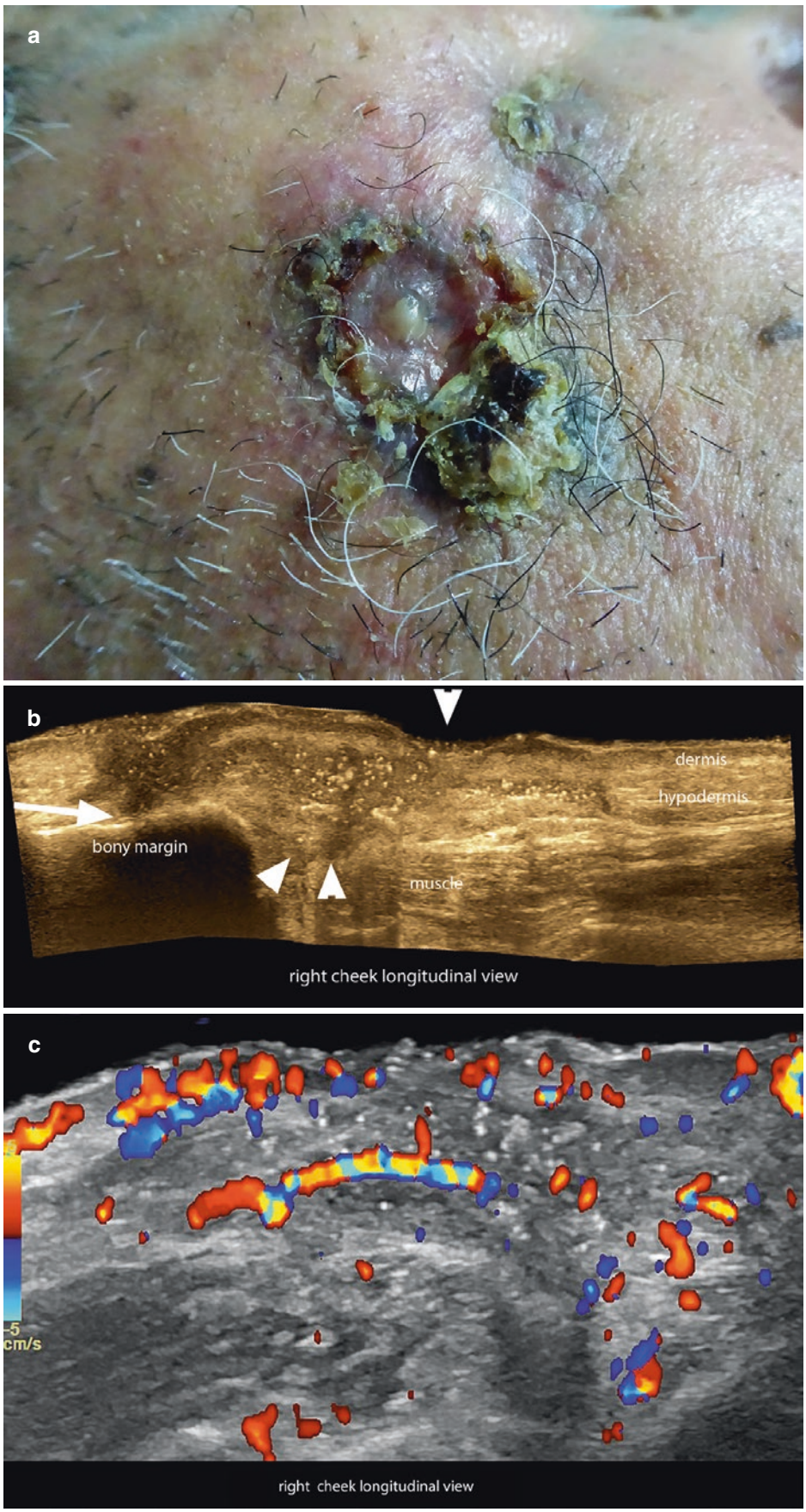

Fig. 5.7 Ulcerated basal cell carcinoma of high-risk-of-recurrence subtype that involves dermis, hypodermis, and the superficial and upper part of the zygomaticus major muscle (*arrowheads*), and contacts the bony margin. (**a**) Clinical photograph. (**b**) Greyscale (with color filter; longitudinal view; right cheek) and (**c**) color Doppler ultrasound demonstrate irregular, hypoechoic structure with spiculated borders and multiple hyperechoic spots suggestive of a high-risk-of-recurrence subtype. Notice in (**b**) the ulceration (*arrowhead pointing downward*), the involvement of the zygomaticus major muscle (*arrowheads pointing upward*) and the contact with the bony margin of the malar bone (*horizontal arrow*). On color Doppler, there is increased vascularity in the dermis, hypodermis, and part of the zygomaticus major muscle.

5.2.2 Squamous Cell Carcinoma

5.2.2.1 Definition

Second most common form of non-melanoma skin cancer. Squamous cell carcinoma (SCC) usually affects areas of the body exposed to the sun, such as the scalp or the face [1–5].

5.2.2.2 Synonyms

Spinocellular carcinoma, epithelioma spinocellulare, spinalioma.

5.2.2.3 Key Sonographic Signs

- Hypoechoic, oval or band-like dermal and/or hypodermal structure (Figs. 5.8, 5.9, and 5.10)
- Usually, SCC does not show hyperechoic spots within the lesion.
- On color Doppler, a moderate increase in the blood flow may be detected within and at the periphery of the lesion.
- Involvement of deeper layers is more common than in BCC.
- Locoregional metastasis of SCC may be detected and can involve the paths of lymphatic drainage of the tumor [5, 6, 15].

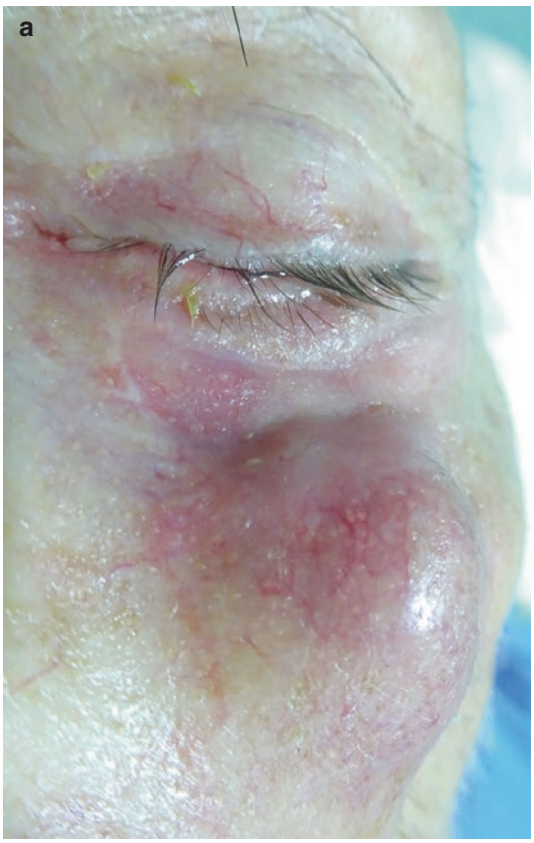

Fig. 5.8 Squamous cell carcinoma with satellite lesions (less than 2 cm from the primary tumor) and perineural involvement. (**a**) Clinical image. (**b** and **c**) Greyscale and color Doppler ultrasound (transverse views; left cheek) shows ill-defined, oval-shaped, hypoechoic dermal and hypodermal solid mass (*asterisk*) that involves the zygomaticus major and minor muscles and presents two well-defined, oval-shaped satellite lesions (*o*), which involve the bony margin and the exit of the infraorbital nerve. On color Doppler, there is prominent vascularity in the periphery and some vessels within the lesion (*asterisk*).

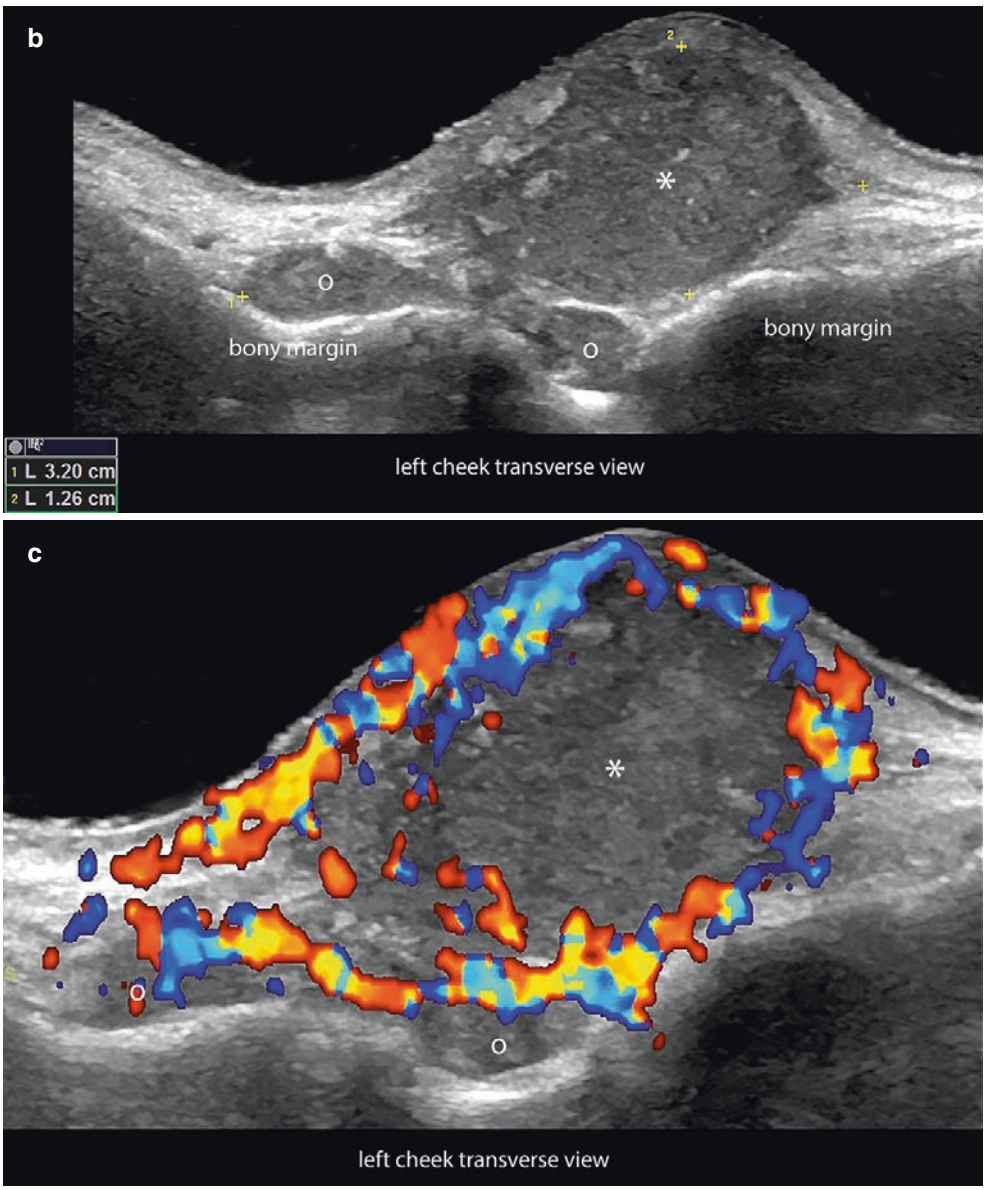

Fig. 5.8 (Continued)

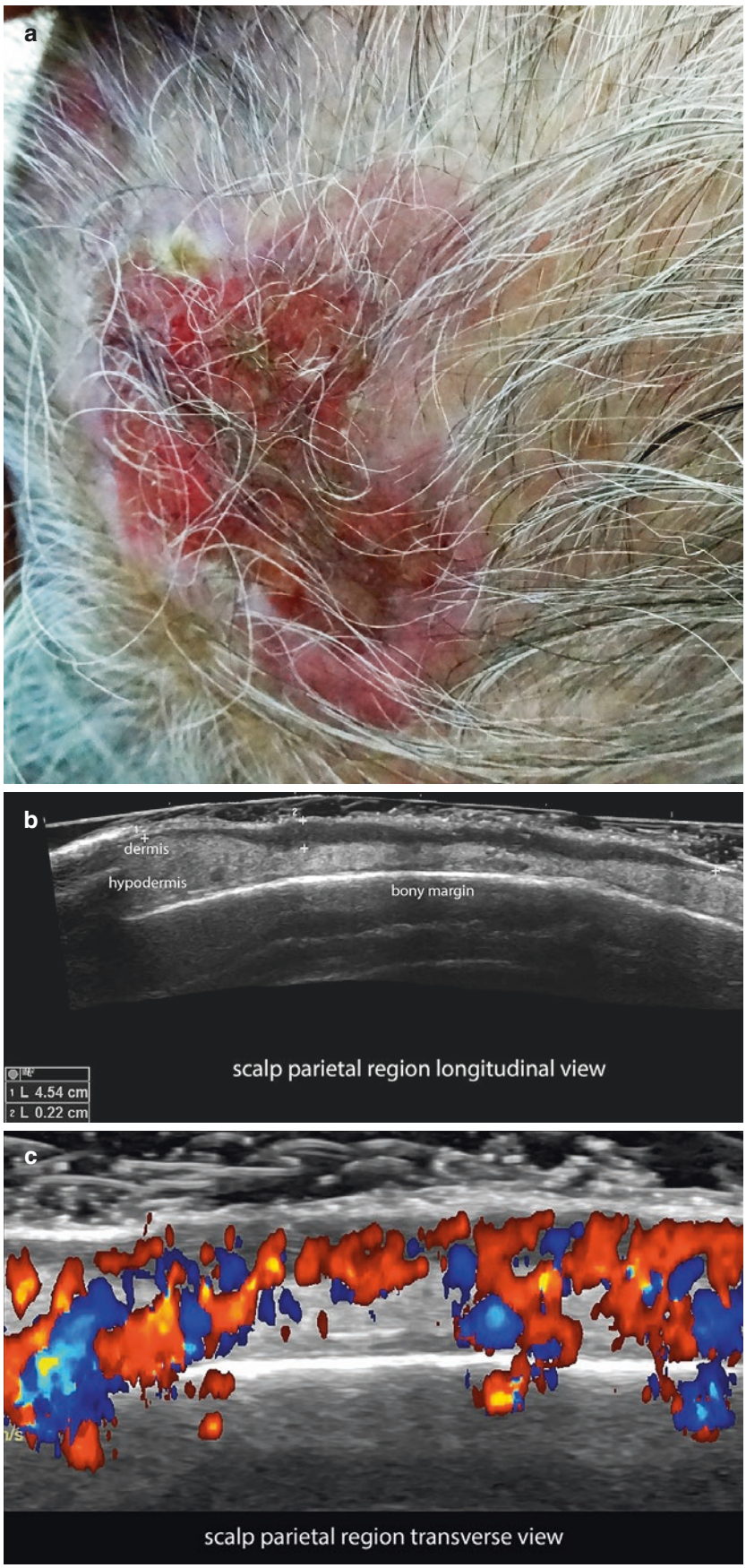

Fig. 5.9 Squamous cell carcinoma of the scalp. (**a**) Clinical photograph. (**b**) Greyscale (longitudinal view) and (**c**) color Doppler ultrasound (transverse view) present a 4.5-cm (major axis) × 0.2-cm (thickness) hypoechoic band that involves dermis and hypodermis.

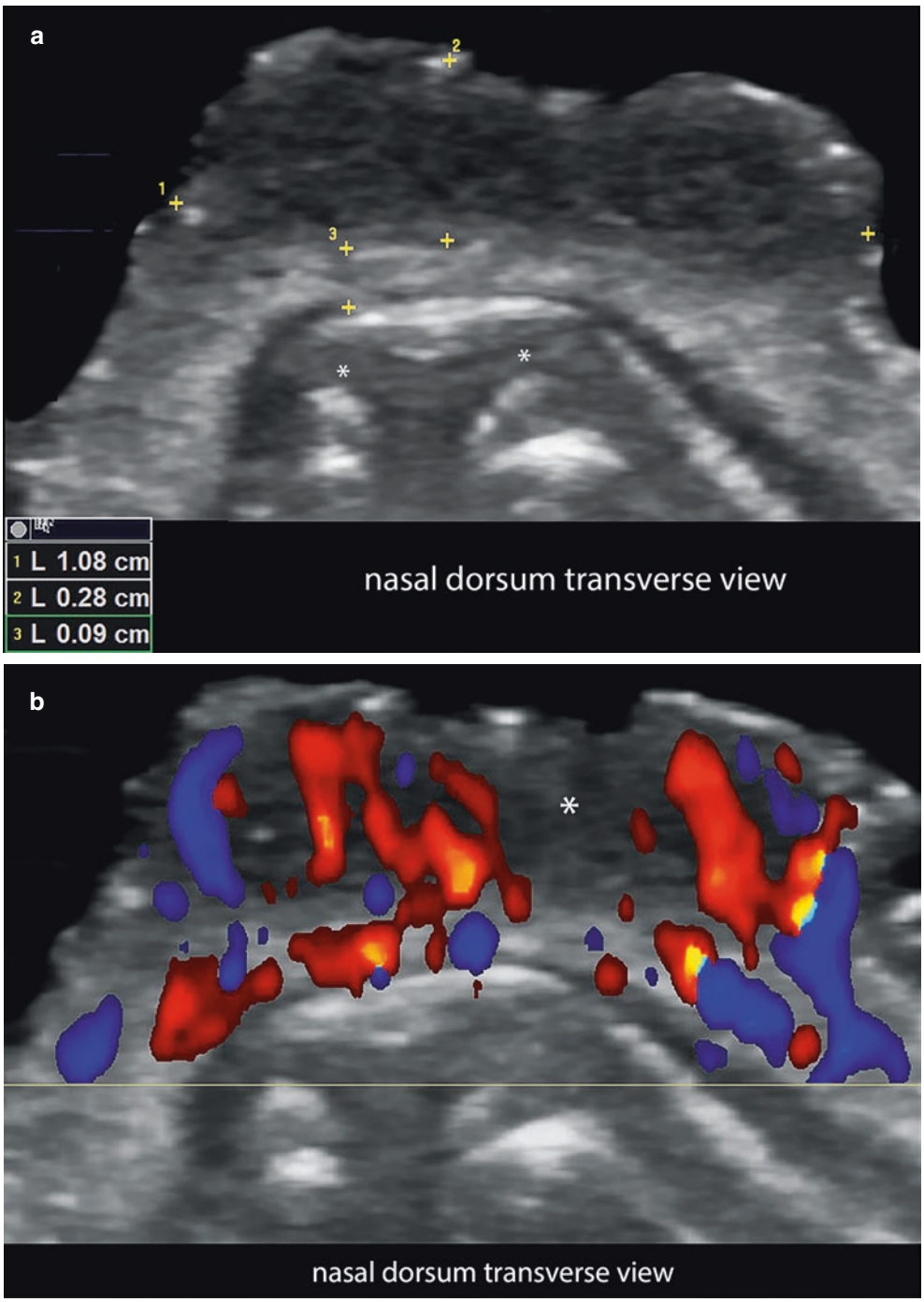

Fig. 5.10 Squamous cell carcinoma of the nasal region. (**a**) Greyscale; and (**b**), color Doppler ultrasound (nasal dorsum; transverse view) demonstrate 1.0-cm (transverse) × 0.3-cm (thickness), ill-defined, hypoechoic lesion (between markers). The deep part of the lesion is located 0.9 mm on top of the nasalis muscle. No signs of involvement of the superior nasal cartilages are seen. On color Doppler, there is increased blood flow within the lesion.

5.3 Melanoma

5.3.1 Definition

Most lethal form of cutaneous cancer, caused by a malignant proliferation of melanocytes. Frequently, malignant melanoma (MM) appears as a hyperpigmented lesion with irregular borders [1, 2, 16].

5.3.2 Synonym

Malignant cutaneous melanoma.

5.3.3 Facts on Melanoma

- The prognosis of the patient with a cutaneous melanoma is strongly related to the histologic thickness of the primary tumor, which has been called the Breslow index (Table 5.1).
- The levels of invasion in melanoma are classified according to Clark's classification (Table 5.2).
- Tumors that measure 1 mm or more in thickness indicate a sentinel lymph node procedure to confirm the degree of locoregional spread.
- Ultrasound can support both the study of the primary lesion (including providing the thickness) and the performance of locoregional staging [16–32].
- Additionally, sonography can help to locate the sentinel lymph node and may guide cytologic (fine-needle aspiration) or histologic procedures.
- Occasionally, melanomas present as non-pigmented lesions; this is called *amelanotic melanoma* and is due to a sarcomatous-like lesion with hidden traces of pigment.
- Melanomas can show satellite metastases (no more than 2 cm from the primary tumor), in-transit metastases (more than 2 cm from the primary tumor), nodal metastases (lymph nodes), and distant metastasis in other organs such as liver, brain, or bone [19–24].

Table 5.1 Breslow's index of thickness of melanoma

Tumor depth, mm	Approximate 5-year survival, %
<1	95–100
1–2	80–96
2.1–4	60–75
>4	50

Table 5.2 Clark's classification of the levels of invasion in melanoma

Levels	Histologic layers
I	In situ melanoma
II	Superficial papillary dermis—subepidermal
III	Superficial and deep papillary dermis abutting the reticular dermis
IV	Papillary and reticular dermis
V	Invasion of the subcutaneous fat

5.3.4 Key Sonographic Signs

- Hypoechoic and commonly fusiform-shaped dermal and/or hypodermal structure
- On color Doppler, prominent hypervascularity is frequently detected within and at the periphery of the tumors (Figs. 5.11 and 5.12).
- Satellite and in-transit metastases usually follow the path of the lymphatic and venous drainage of the tumor and appear as oval-shaped, hypoechoic hypodermal structures commonly surrounded by hyperechoic hypodermal fatty tissue. Melanoma metastasis commonly shows hypervascularity on color Doppler.
- Satellite, in-transit, and nodal metastasis may present anechoic areas that have been associated with the presence of compact nests of malignant cells and are not due to intratumoral necrosis.
- Ultrasound can support fine-needle aspiration and biopsy for melanoma.
- An ultrasound-guided sentinel lymph node procedure can be performed [16–32].

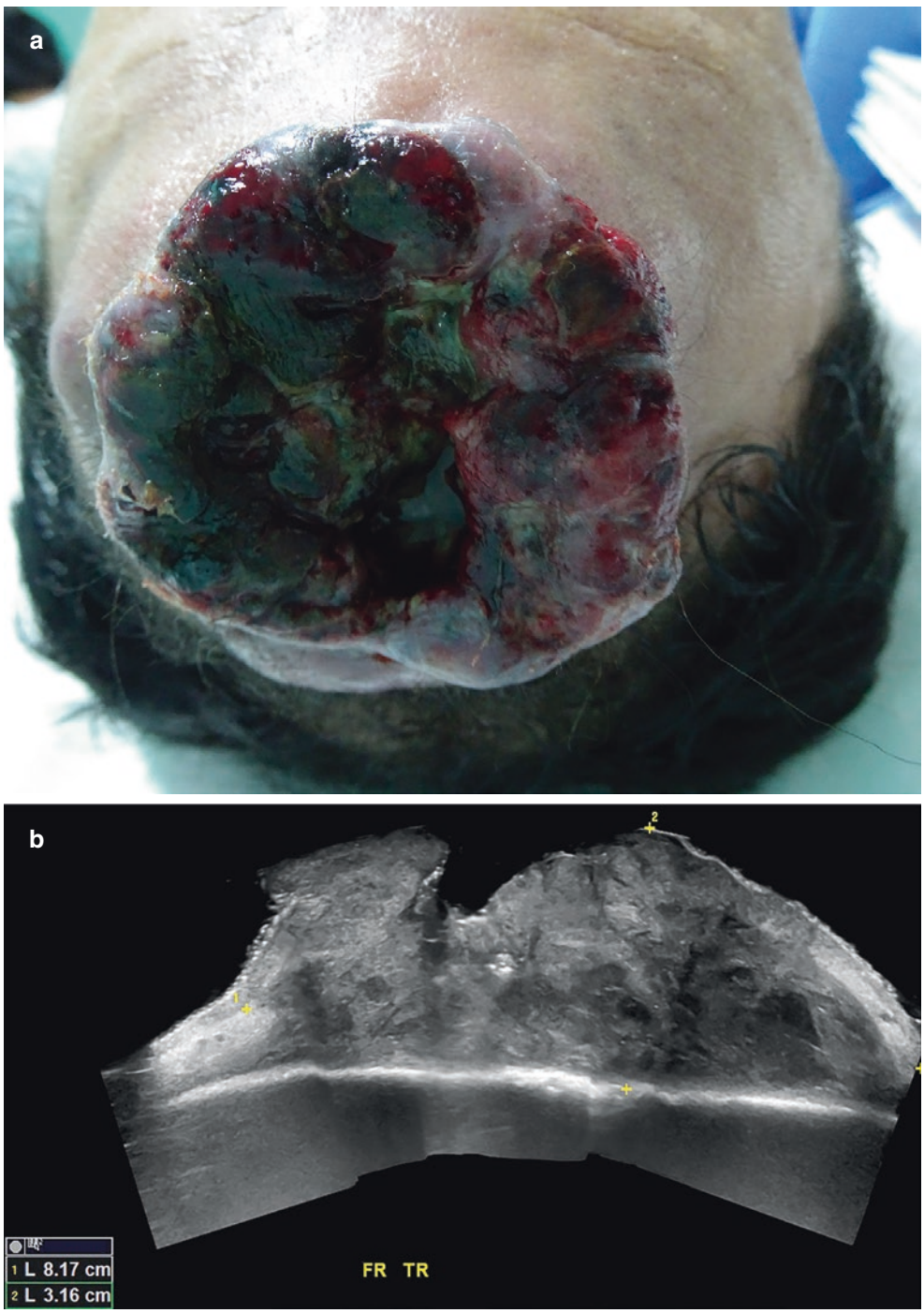

Fig. 5.11 Melanoma in the scalp at an advanced stage. (**a**) Clinical image; (**b**) Greyscale panoramic ultrasound (transverse view); and (**c**) color Doppler ultrasound (longitudinal view) demonstrate 8.2-cm (transverse) × 3.2-cm (thickness) ill-defined, irregular, hypoechoic mass that involves dermis, hypodermis, and the musculoaponeurotic layer. On color Doppler, there is increased blood flow within the lesion.

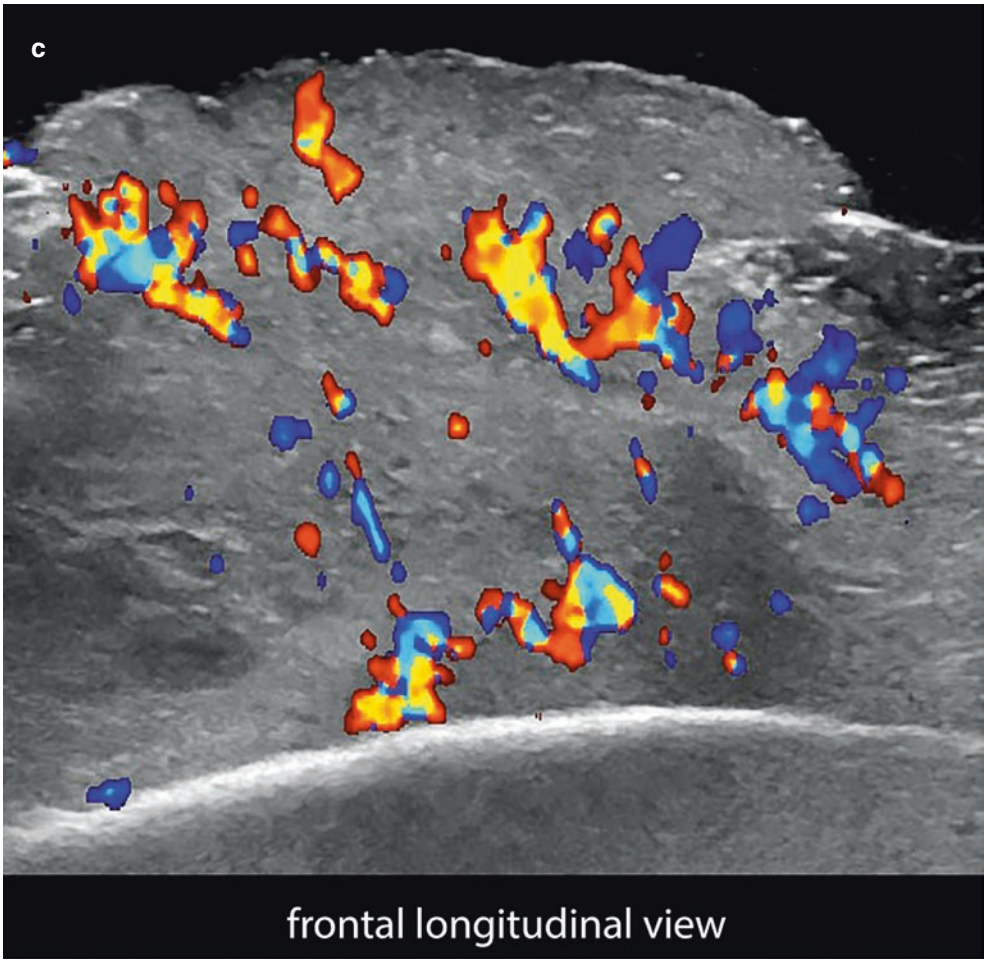

Fig. 5.11 (Continued)

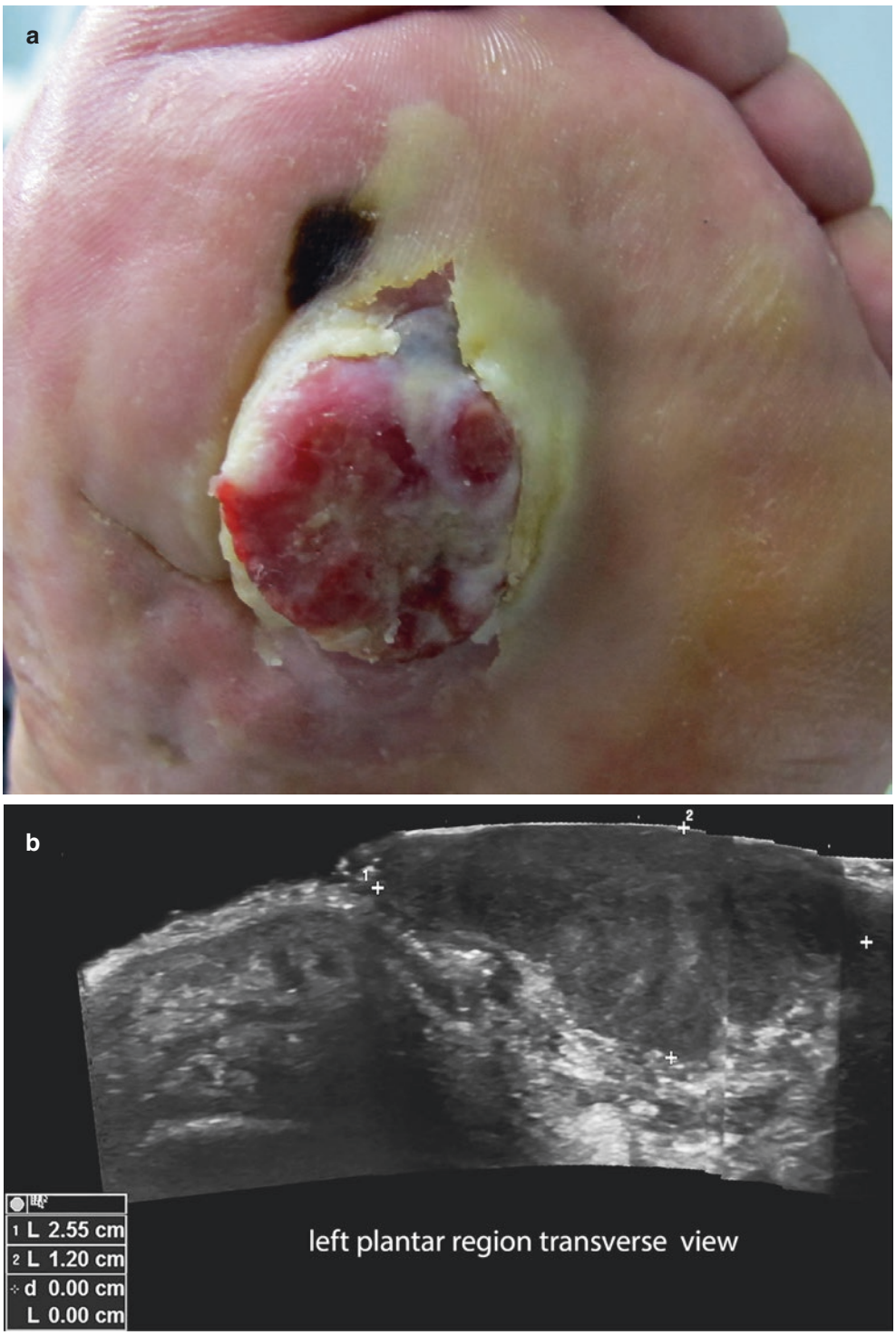

Fig. 5.12 Plantar melanoma. (**a**) Clinical photograph of mostly amelanotic melanoma (**b** and **c**) Greyscale and color Doppler ultrasound (transverse views) show ill-defined, hypoechoic mass that involves dermis and hypodermis. On color Doppler, prominent vascularity is detected within the lesion.

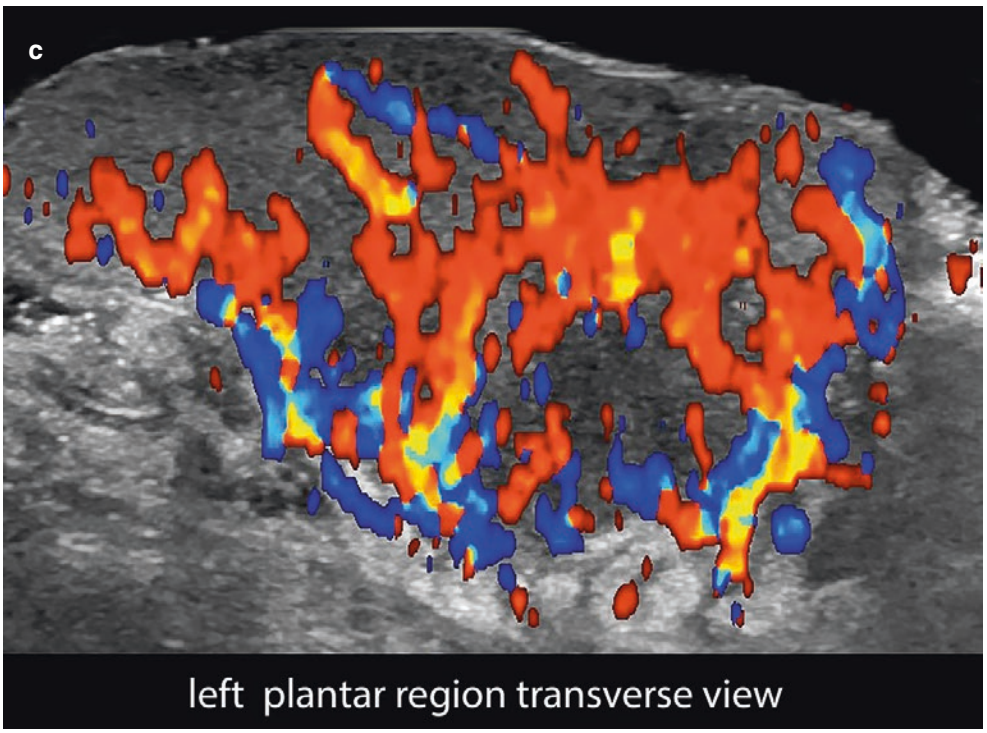

Fig. 5.12 (Continued)

5.4 Dermatofibrosarcoma Protuberans (DFSP)

5.4.1 Definition

Intermediate to lowgrade of fibrous sarcomatous tumor that shows high rates of local recurrence and low risk of metastasis. DFSP occurs most commonly in the trunk and proximal extremities but may also affect other regions, such as the face and neck.

5.4.2 Key Sonographic Signs

- Ill-defined, mixed-echogenicity mass with a hypoechoic band-like or nodular dermal and/or hypodermal superficial part and a hyperechoic hypodermal region that present convex borders or pseudopods-like areas [5, 33–37].
- The degree of vascularity within the lesion varies; lesions tend to show a moderate presence of low-velocity arterial and venous vessels (Figs. 5.13 and 5.14).
- DFSP can involve the fascial and muscular layers and may present satellite metastases (i.e., located at no more than 2 cm from the primary tumor), which appear as hypoechoic nodules in the vicinity of the lesion.

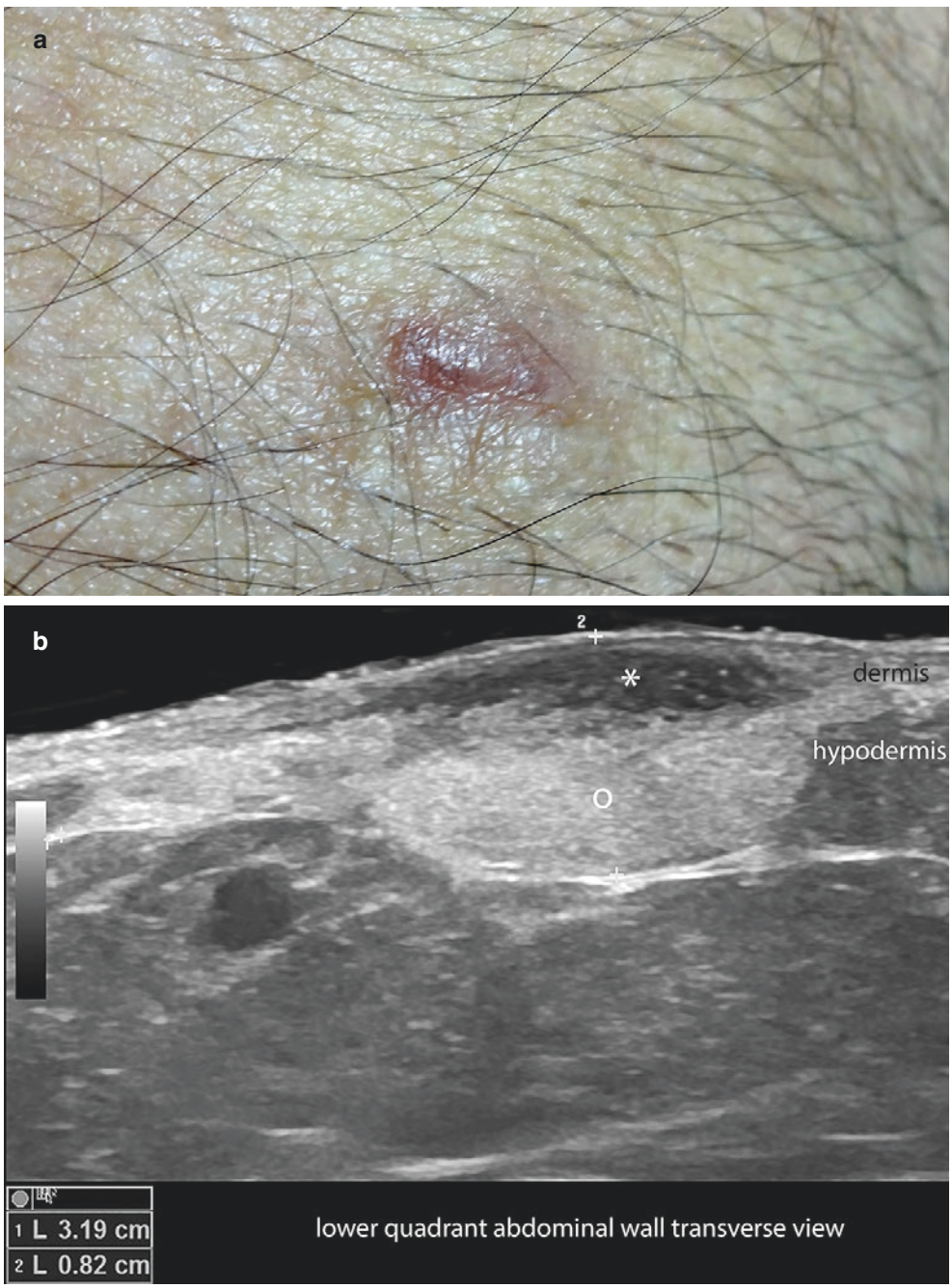

Fig. 5.13 Dermatofibrosarcoma protuberans. (**a**) Clinical image in the right lower quadrant of the abdominal wall with a lesion that simulated a keloid. (**b**) Greyscale (transverse view); (**c**) power Doppler; and (**d**) 3D reconstruction ultrasound demonstrate a structure with mixed echogenicity, upper hypoechogenicity (*asterisk*) of the dermis and some part of the upper hypodermis, and a deeper hyperechogenicity (*o*) of the hypodermal part. Notice the lobulated and convex borders at the deep part of the tumor. On power Doppler, increased vascularity within the lesion predominates in the upper part.

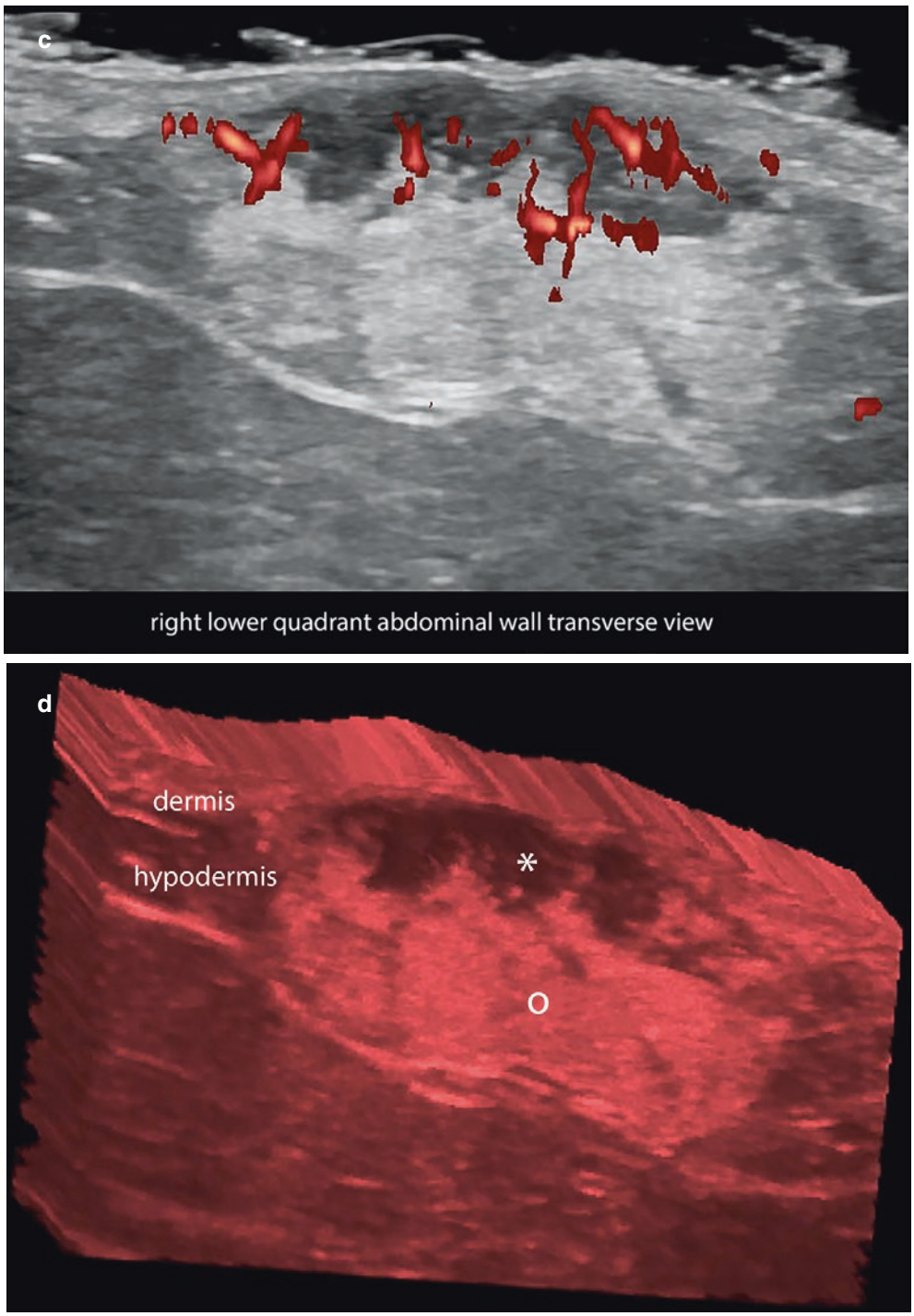

Fig. 5.13 (Continued)

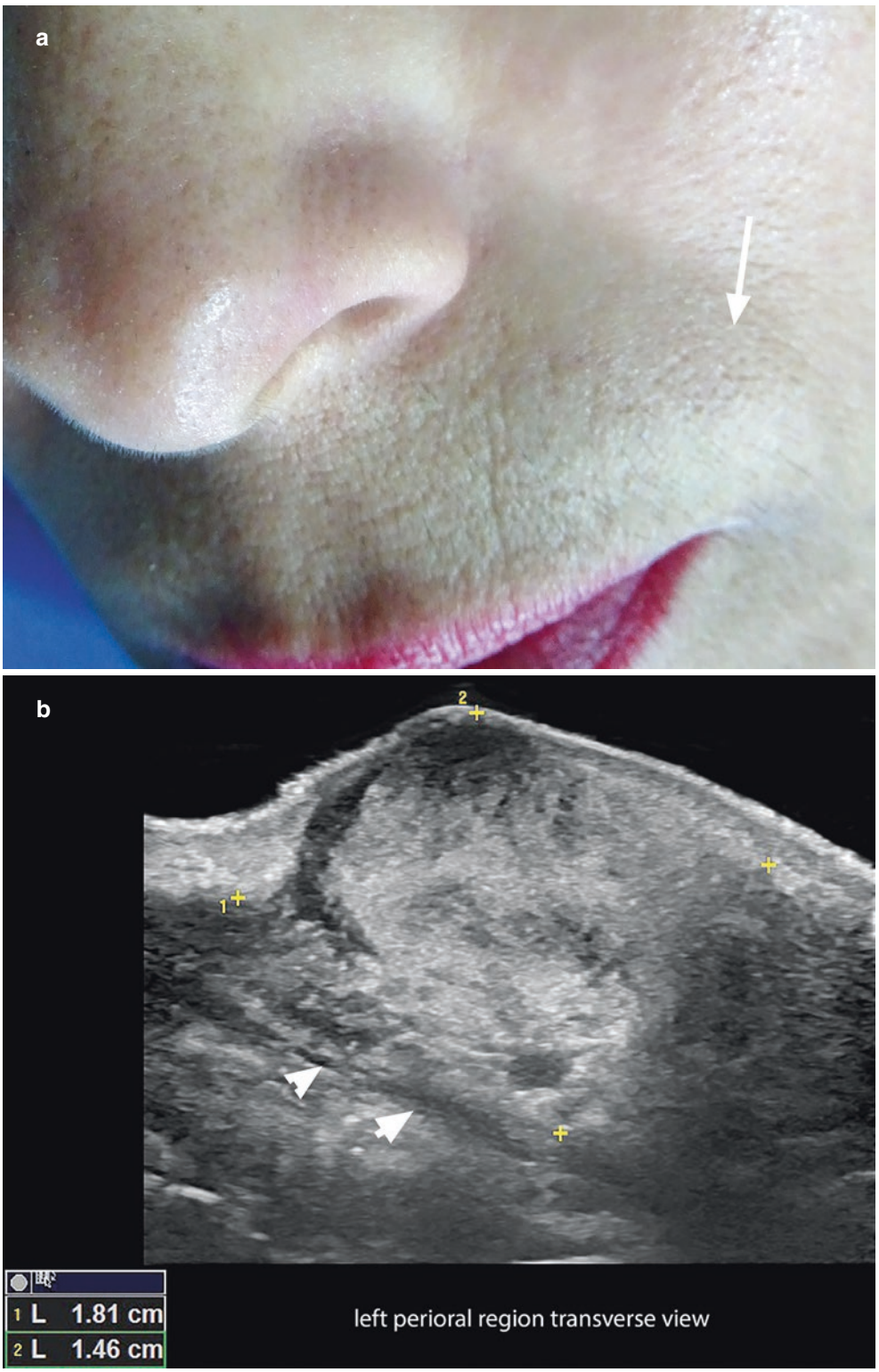

Fig. 5.14 Dermatofibrosarcoma protuberans. (**a**) Clinical photograph of a lump in the left perioral region. (**b** and **c**) Greyscale and color Doppler ultrasound (transverse views) demonstrates 1.8-cm (transverse) × 1.5-cm (thickness) ill-defined, oval-shaped, mixed echogenicity dermal and hypodermal mass. Notice the lower echogenicity in the upper part and the hyperechogenicity at the deeper part. There is infiltration of the left border of the orbicularis oris muscle (*arrowheads*). On color Doppler, there is more intense hypervascularity at the upper part of the mass.

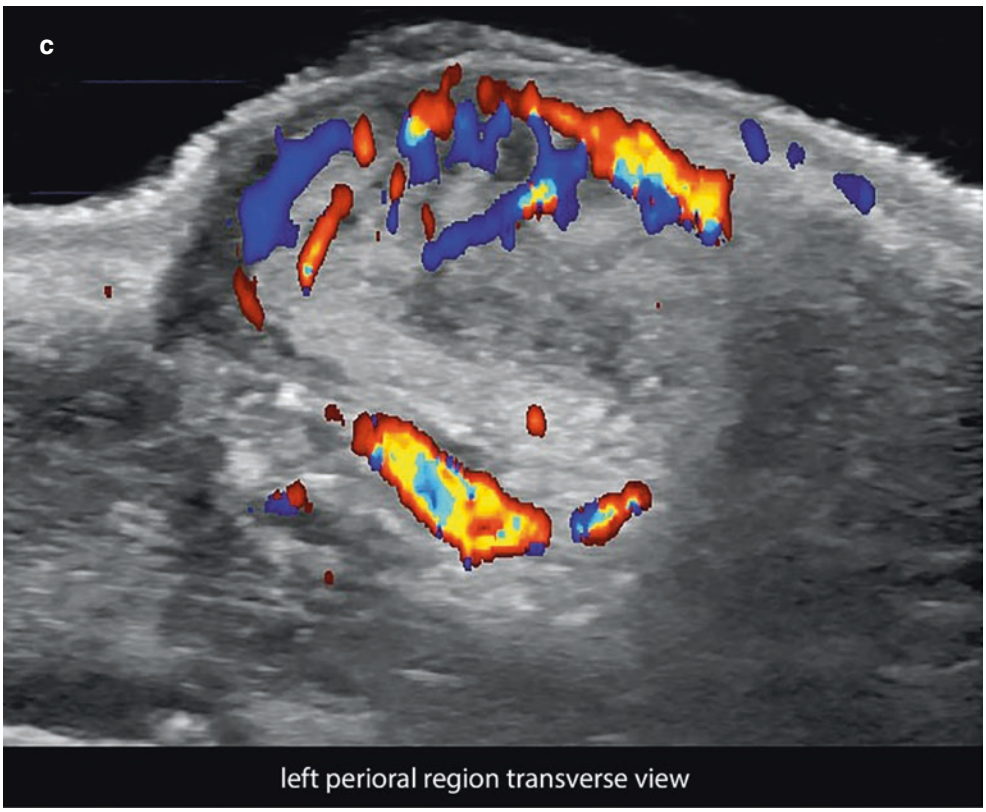

Fig. 5.14 (Continued)

5.5 Merkel Cell Carcinoma

5.5.1 Definition

Aggressive form of cutaneous cancer, frequently lethal, that presents fast growth.

5.5.2 Key Sonographic Signs

- Ill-defined hypoechoic dermal and/or hypodermal tumor that shows intense hypervascularity on color Doppler (Fig. 5.15) [38, 39].
- The tumor can invade deeper layers such as muscle or bone.

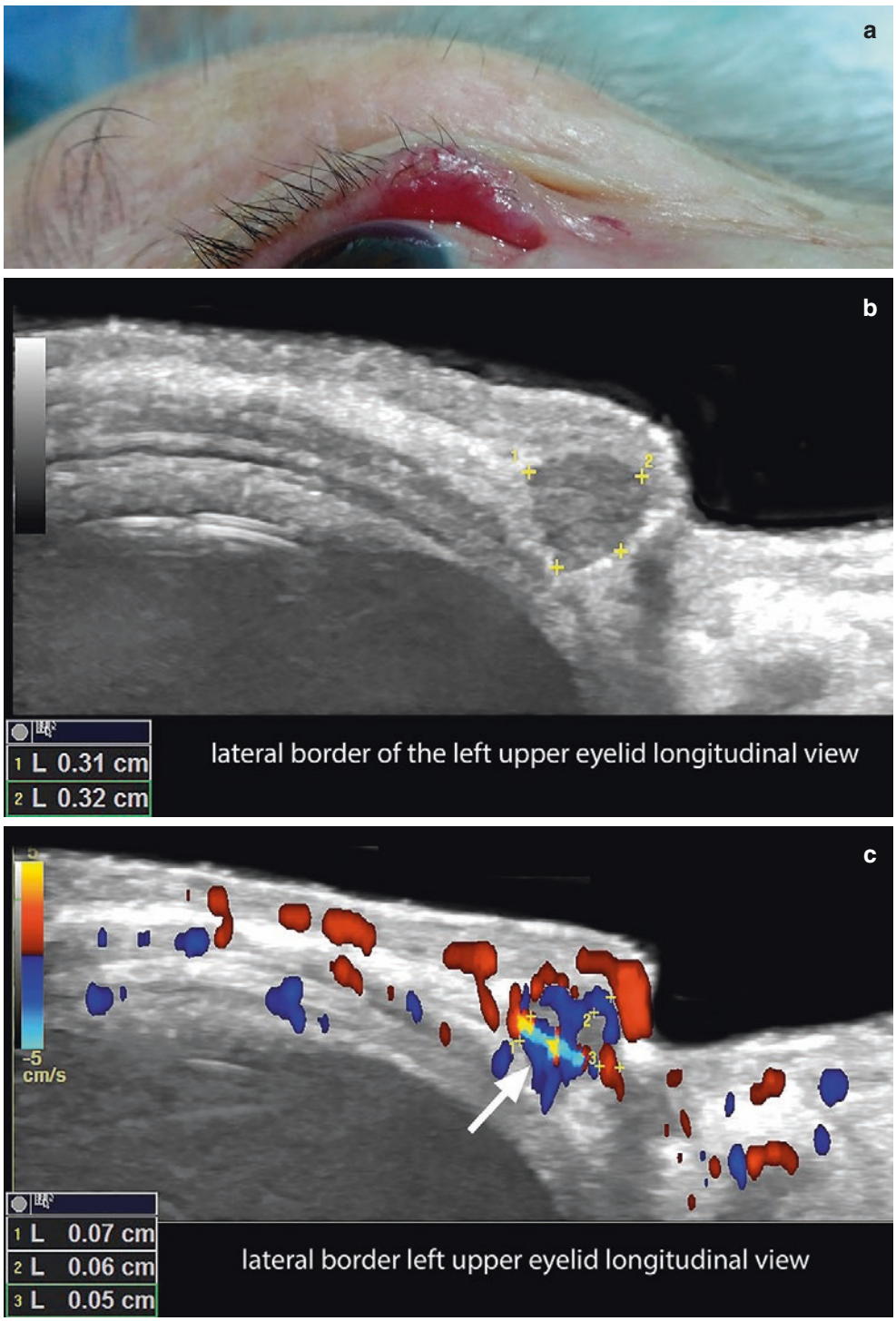

Fig. 5.15 Merkel cell carcinoma (**a**) Clinical photograph. (**b** and **c**) Greyscale and color Doppler ultrasound show 3.1-mm (longitudinal) × 3.2-mm (thickness), oval-shaped hypoechoic nodule that involves the lower dermal border of the lateral aspect of the upper eyelid. On color Doppler, there is prominent blood flow in the periphery and within the lesion. The thickness of the vessels varies between 0.5 mmand 0.7 mm.

5.6 Malignant Lymph Nodes

5.6.1 Definition

Infiltration of lymph nodes by neoplastic cells.

5.6.2 Key Sonographic Signs

- **Normal or benign lymph nodes** show as oval-shaped nodules with a thin and well-defined hypoechoic cortex and hyperechoic medulla. The vascular hilum is usually located in one of the borders of the lymph node, and the main vascular branches are mainly located in the medulla (Fig. 5.16). Benign inflammatory or reactive lymph nodes may show thickening of the cortex; however, they maintain the main sonographic features of normal lymph nodes.
- **Signs of malignancy in lymph nodes** (Figs. 5.17 and 5.18):
  - Round shape
  - Partial or total loss of the difference in echogenicity between the cortex and the medulla of the lymph node
  - Cortical hypoechoic nodules or asymmetrical areas with increased thickness of the cortex
  - Diffusely hypoechoic lymph node
  - Increased echogenicity of the hypodermis in the periphery of the lymph node
  - Size greater than 1 cm (transverse axis)—through lymph nodes in some areas (such as the jugulodigastric, axillary and groin areas) normally present a larger size
  - On color Doppler, prominent cortical or diffuse blood flow with tortuous, irregular, and/or thick vessels [40–49].
- Ultrasound-guided fine-needle aspiration and/or biopsy may support the diagnosis
- Qualitative and quantitative elastography have been reported to support the diagnosis of malignancy, with higher sensitivity in quantitative elastography (shear wave).

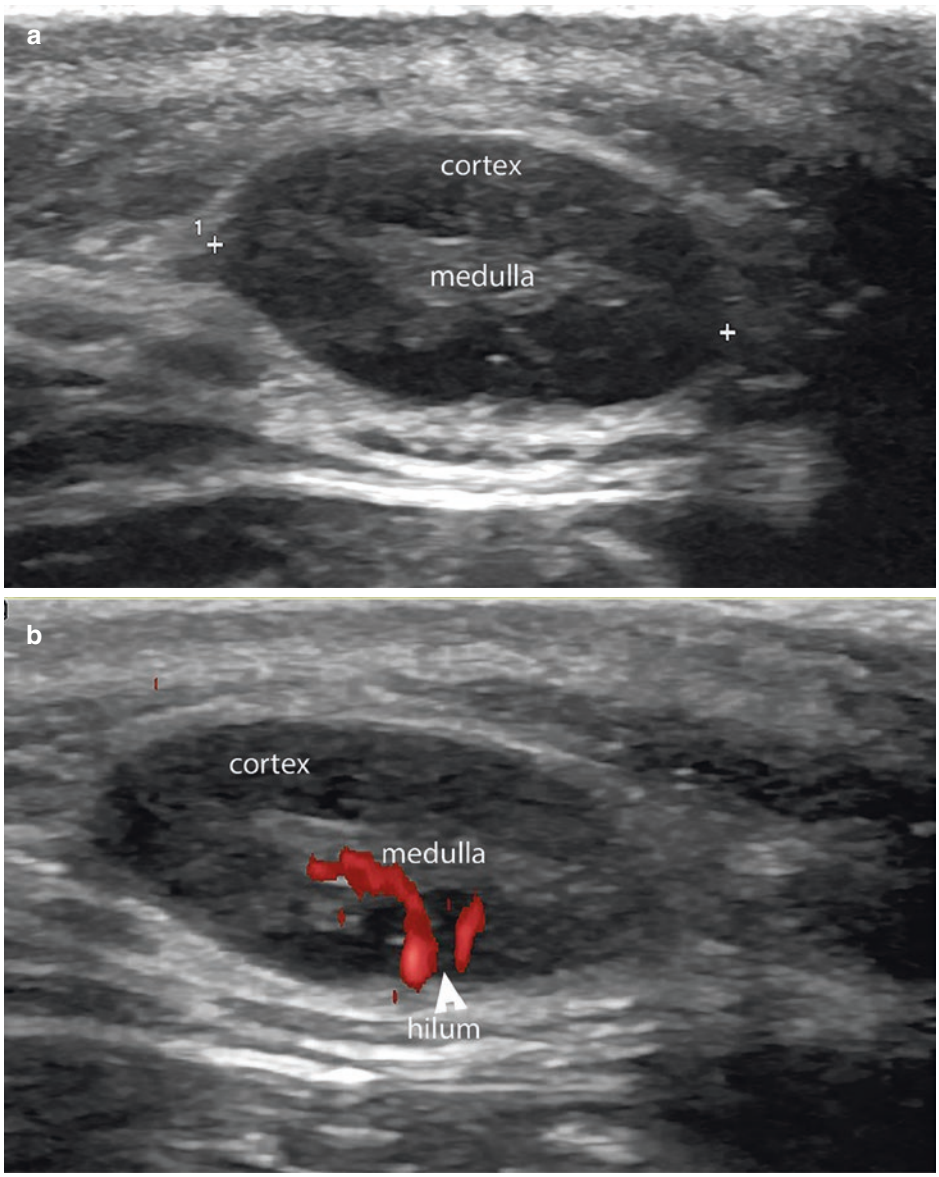

Fig. 5.16 Ultrasonographic morphology of benign lymph nodes. (**a**) Greyscale. (**b**) Color Doppler shows well-defined, oval-shaped structures with an outer hypoechoic cortex and inner hyperechoic medulla. In (**b**) the vascular hilum is located in a border and the vascularity tends to be centripetal.

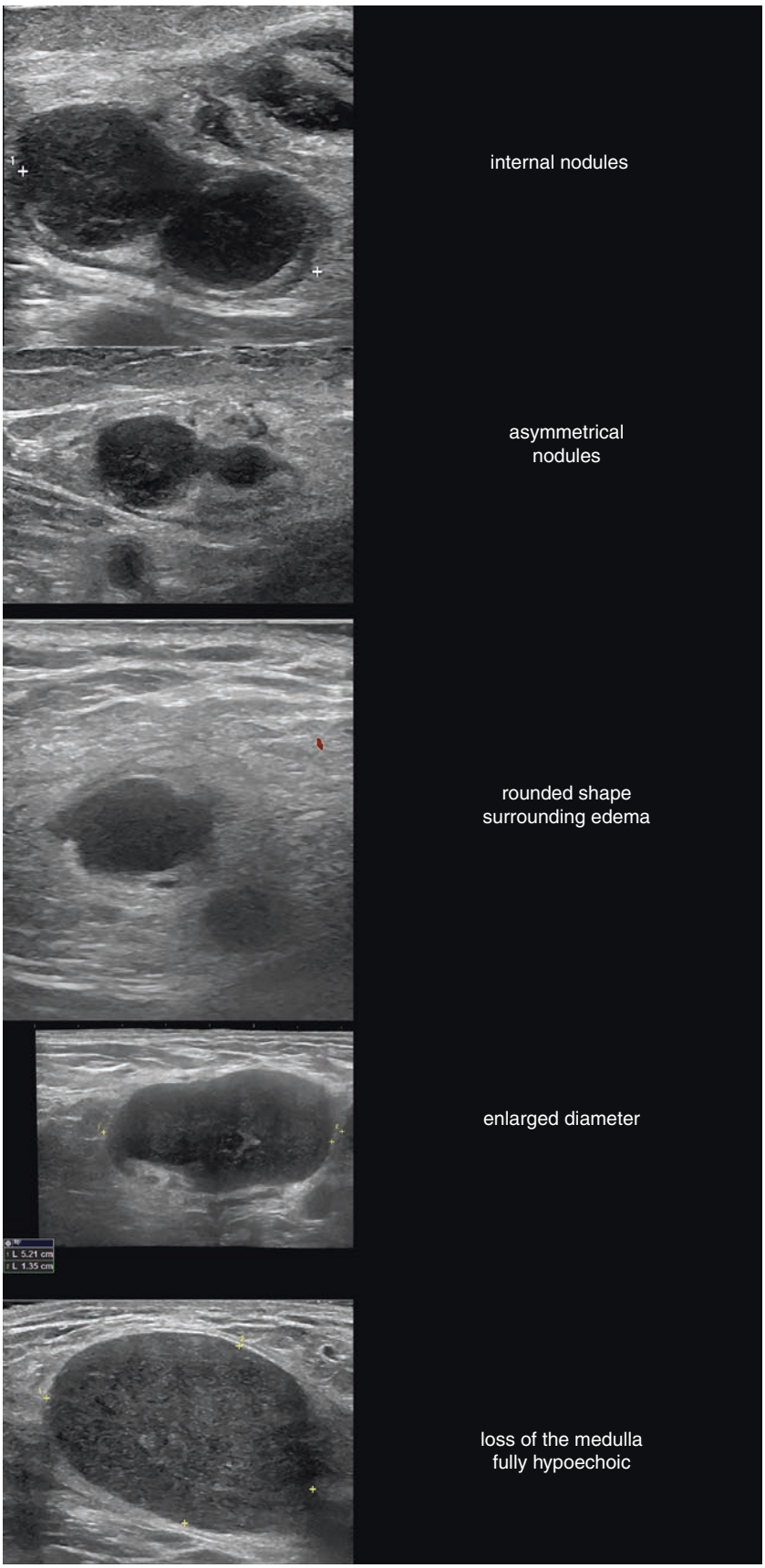

Fig. 5.17 Ultrasound morphologies in greyscale, suggestive of malignant lymph nodes.

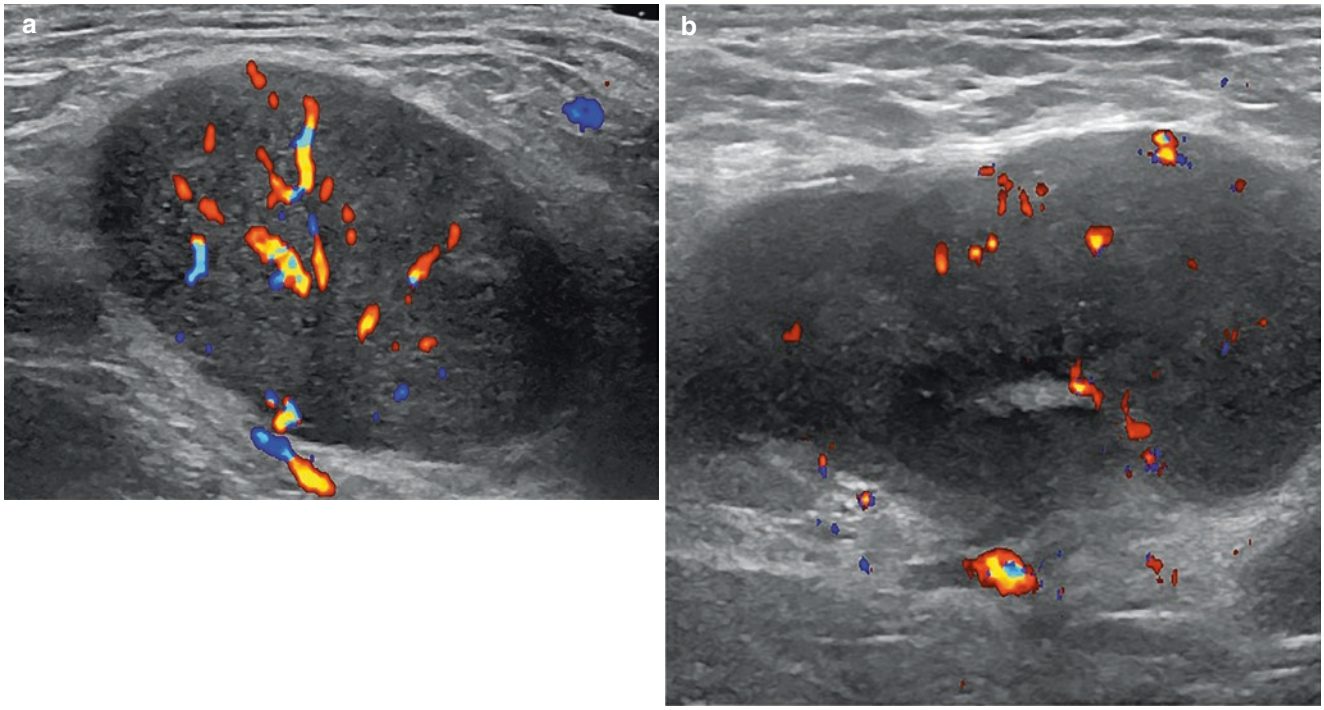

Fig. 5.18 Patterns of peripheral blood flow of malignant lymph nodes. (**a**) Low degree of peripheral vascularity. (**b**) High degree of peripheral vascularity.

References

1. Rogers HW, Weinstock MA, Feldman SR, Coldiron BM. Incidence estimate of nonmelanoma skin cancer (keratinocyte carcinomas) in the US population, 2012. JAMA Dermatol. 2015;151:1081–6.
2. American Cancer Society. Cancer facts and figures 2017. Atlanta: American Cancer Society; 2017. http://www.cancer.org/acs/groups/content/@editorial/documents/document/acspc-048738.pdf. Accessed 5 Dec 2017.
3. Lear W, Dahlke E, Murray CA. Basal cell carcinoma: review of epidemiology, pathogenesis, and associated risk factors. J Cutan Med Surg. 2007;11:19–30.
4. Kwasniak LA, Garcia-Zuazaga J. Basal cell carcinoma: evidence-based medicine and review of treatment modalities. Int J Dermatol. 2011;50:645–58.
5. Wortsman X, Carreño L, Morales C. Skin cancer: the primary tumors. In: Wortsman X, Jemec GBE, editors. Dermatologic ultrasound with clinical and histologic correlations. New York: Springer; 2013. p. 249–82.
6. MacFarlane D, Shah K, Wysong A, Wortsman X, Humphreys TR. The role of imaging in the management of patients with non-melanoma skin cancer. J Am Acad Dermatol. 2017;76:579–88.
7. Wortsman X, Vergara P, Castro A, Saavedra D, Bobadilla F, Sazunic I, et al. Ultrasound as predictor of histologic subtypes linked to recurrence in basal cell carcinoma of the skin. J Eur Acad Dermatol Venereol. 2015;29:702–7.
8. Wortsman X. Sonography of facial cutaneous basal cell carcinoma: a first-line imaging technique. J Ultrasound Med. 2013;32:567–72.
9. Vega N, Wortsman X, Navarrete N, Sazunic I. Color Doppler ultrasound supports early diagnosis of mixed high and low risk of recurrence subtypes in the same basal cell carcinoma lesion. Dermatol Surg. 2017. https://doi.org/10.1097/DSS.0000000000001328. [Epub ahead of print].
10. Bobadilla F, Wortsman X, Muñoz C, Segovia L, Espinoza M, Jemec GB. Pre-surgical high resolution ultrasound of facial basal cell carcinoma: correlation with histology. Cancer Imaging. 2008;8:163–72.
11. Hernández-Ibáñez C, Blazquez-Sánchez N, Aguilar-Bernier M, Fúnez-Liébana R, Rivas-Ruiz F, de Troya-Martín M. Usefulness of high-frequency ultrasound in the classification of histologic subtypes of primary basal cell carcinoma. Actas Dermosifiliogr. 2017;108:42–51.
12. Pasquali P, Freites-Martinez A, Fortuño-Mar A. Ex vivo high-frequency ultrasound: A novel proposal for management of surgical margins in patients with non-melanoma skin cancer. J Am Acad Dermatol. 2016;74:1278–80.
13. Barcaui Ede O, Carvalho AC, Valiante PM, Barcaui CB. High-frequency ultrasound associated with dermoscopy in pre-operative evaluation of basal cell carcinoma. An Bras Dermatol. 2014;89:828–31.
14. Hernández-Ibáñez C, Aguilar-Bernier M, Fúnez-Liébana R, Del Boz J, Blázquez N, de Troya M. The usefulness of high-resolution ultrasound in detecting invasive disease in recurrent basal cell carcinoma after nonsurgical treatment. Actas Dermosifiliogr. 2014;105:935–9.
15. Ruiz ES, Karia PS, Morgan FC, Schmults CD. The positive impact of radiologic imaging on high-stage cutaneous squamous cell carcinoma management. J Am Acad Dermatol. 2017;76:217–25.
16. Nazarian LN, Alexander AA, Rawool NM, Kurtz AB, Maguire HC, Mastrangelo MJ. Malignant melanoma: impact of superficial US on management. Radiology. 1996;199:273–7.
17. Nazarian LN, Alexander AA, Kurtz AB, Capuzzi DM Jr, Rawool NM, Gilbert KR, Mastrangelo MJ. Superficial melanoma metastases: appearances on gray-scale and color Doppler sonography. AJR Am J Roentgenol. 1998;170:459–63.

18. Forsberg F, Ro RJ, Liu JB, Lipcan KJ, Potoczek M, Nazarian LN. Monitoring angiogenesis in human melanoma xenograft model using contrast-enhanced ultrasound imaging. Ultrason Imaging. 2008;30:237–46.
19. Catalano O, Caracò C, Mozzillo N, Siani A. Locoregional spread of cutaneous melanoma: sonography findings. AJR Am J Roentgenol. 2010;194:735–45.
20. Catalano O, Setola SV, Vallone P, Raso MM, D'Errico AG. Sonography for locoregional staging and follow-up of cutaneous melanoma: how we do it. J Ultrasound Med. 2010;29:791–802.
21. Catalano O. Critical analysis of the ultrasonographic criteria for diagnosing lymph node metastasis in patients with cutaneous melanoma: a systematic review. J Ultrasound Med. 2011;30:547–60.
22. Catalano O, Voit C, Sandomenico F, Mandato Y, Petrillo M, Franco R, et al. Previously reported sonographic appearances of regional melanoma metastases are not likely due to necrosis. J Ultrasound Med. 2011;30:1041–9.
23. Marone U, Catalano O, Caracò C, Anniciello AM, Sandomenico F, Di Monta G, et al. Can high-resolution ultrasound avoid the sentinel lymph-node biopsy procedure in the staging process of patients with stage I-II cutaneous melanoma? Ultraschall Med. 2012;33:E179–85.
24. Wortsman X. Sonography of the primary cutaneous melanoma: a review. Radiol Res Pract. 2012;2012:814396.
25. Crisan M, Crisan D, Sannino G, Lupsor M, Badea R, Amzica F. Ultrasonographic staging of cutaneous malignant tumors: an ultrasonographic depth index. Arch Dermatol Res. 2013;305:305–13.
26. Badea R, Crişan M, Lupşor M, Fodor L. Diagnosis and characterization of cutaneous tumors using combined ultrasonographic procedures (conventional and high resolution ultrasonography). Med Ultrason. 2010;12:317–22.
27. Fernández Canedo I, de Troya Martín M, Fúnez Liébana R, Rivas Ruiz F, Blanco Eguren G, Blázquez Sánchez N. Preoperative 15-MHz ultrasound assessment of tumor thickness in malignant melanoma. Actas Dermosifiliogr. 2013;104:227–31.
28. Music MM, Hertl K, Kadivec M, Pavlović MD, Hocevar M. Preoperative ultrasound with a 12–15 MHz linear probe reliably differentiates between melanoma thicker and thinner than 1 mm. J Eur Acad Dermatol Venereol. 2010;24:1105–8.
29. Lassau N, Mercier S, Koscielny S, Avril MF, Margulis A, Mamelle G, et al. Prognostic value of high-frequency sonography and color Doppler sonography for the preoperative assessment of melanomas. AJR Am J Roentgenol. 1999;172:457–61.
30. Lassau N, Koscielny S, Avril MF, Margulis A, Duvillard P, De Baere T, et al. Prognostic value of angiogenesis evaluated with high-frequency and color Doppler sonography for preoperative assessment of melanomas. AJR Am J Roentgenol. 2002;178:1547–51.
31. Lassau N, Spatz A, Avril MF, Tardivon A, Margulis A, Mamelle G, et al. Value of high-frequency US for preoperative assessment of skin tumors. Radiographics. 1997;17:1559–65.
32. Voit C, Van Akkooi AC, Schäfer-Hesterberg G, Schoengen A, Kowalczyk K, Roewert JC, et al. Ultrasound morphology criteria predict metastatic disease of the sentinel nodes in patients with melanoma. J Clin Oncol. 2010;28:847–52.
33. Llombart B, Serra-Guillén C, Monteagudo C, López Guerrero JA, Sanmartín O. Dermatofibrosarcoma protuberans: a comprehensive review and update on diagnosis and management. Semin Diagn Pathol. 2013;30:13–28.
34. Sung TH, Tam AC, Khoo JL. Dermatofibrosarcoma protuberans: a comprehensive review on the spectrum of clinico-radiological presentations. J Med Imaging Radiat Oncol. 2017;61:9–17.
35. Bae SH, Lee JY. Imaging features of breast dermatofibrosarcoma protuberans in various modalities including FDG-PET CT. Iran J Radiol. 2016;13:e33916.
36. Zhang L, Liu QY, Cao Y, Zhong JS, Zhang WD. Dermatofibrosarcoma protuberans: computed tomography and magnetic resonance imaging findings. Medicine (Baltimore). 2015;94:e1001.
37. Shin YR, Kim JY, Sung MS, Jung JH. Sonographic findings of dermato fibrosarcoma protuberans with pathologic correlation. J Ultrasound Med. 2008;27:269–74.
38. Catalano O, Alfageme Roldán F, Scotto di Santolo M, Solivetti FM, Wortsman X. Color Doppler sonography of Merkel cell carcinoma. J Ultrasound Med. 2018;37:285–92. https://doi.org/10.1002/jum.14329.
39. Hernández-Aragüés I, Vázquez-Osorio I, Alfageme F, Ciudad-Blanco C, Casas-Férnandez L, Rodríguez-Blanco MI, Suárez-Fernández R. Skin ultrasound features of Merkel cell carcinoma. J Eur Acad Dermatol Venereol. 2017;31:e315–8.
40. Ying M, Bhatia KS, Lee YP, Yuen HY, Ahuja AT. Review of ultrasonography of malignant neck nodes: greyscale, Doppler, contrast enhancement and elastography. Cancer Imaging. 2014;13:658–69.
41. Vassallo P, Wernecke K, Roos N, Peters PE. Differentiation of benign from malignant superficial lymphadenopathy: the role of high-resolution US. Radiology. 1992;183:215–20.
42. Ying M, Ahuja A, Brook F, Metreweli C. Power Doppler sonography of normal cervical lymph nodes. J Ultrasound Med. 2000;19:511–7.
43. Dragoni F, Cartoni C, Pescarmona E, Chiarotti F, Puopolo M, Orsi E, et al. The role of high resolution pulsed and color Doppler ultrasound in the differential diagnosis of benign and malignant lymphadenopathy: results of multivariate analysis. Cancer. 1999;85:2485–90.
44. Chang DB, Yuan A, Yu CJ, Luh KT, Kuo SH, Yang PC. Differentiation of benign and malignant cervical lymph nodes with color Doppler sonography. AJR Am J Roentgenol. 1994;162:965–8.
45. Adibelli ZH, Unal G, Gul E, Uslu F, Kocak U, Abali Y. Differentiation of benign and malignant cervical lymph nodes: value of B-mode and color Doppler sonography. Eur J Radiol. 1998;28:230–4.
46. Ying L, Hou Y, Zheng HM, Lin X, Xie ZL, Hu YP. Real-time elastography for the differentiation of benign and malignant superficial lymph nodes: a meta-analysis. Eur J Radiol. 2012;81:2576–84.
47. Wortsman X, Azocar P, Bouffard JA. Conditions that can mimic dermatologic diseases. In: Wortsman X, Jemec GBE, editors. Dermatologic ultrasound with clinical and histologic correlations. New York: Springer; 2013. p. 505–69.
48. Wortsman X, Revuz J, Jemec GBE. Lymph nodes in hidradenitis suppurativa. Dermatology. 2009;219:32–41.
49. Prativadi R, Dahiya N, Kamaya A, Bhatt S. Chapter 5 ultrasound characteristics of benign vs malignant cervical lymph nodes. Semin Ultrasound CT MR. 2017;38:506–15.